RSV infection is limited to the most superficial layer of polarized, ciliated cells in the respiratory tract epithelium, entering through the apical surface (Zhang *et al.*, 2002; Wright *et al.*, 2005). Late steps of the RSV life cycle include assembly and budding of the virus, which also occur at the apical membrane in polarized cells (Roberts *et al.*, 1995). RSV replicates in the airway mucosa, where it may produce uncomplicated upper respiratory infection or spread distally to the lower airways, producing more severe lower respiratory tract infection. The mechanisms of entry, replication, and budding of RSV, however, are still unclear in the upper airway, including in the nasal mucosa.

Many signaling molecules are considered major players in RSV-induced respiratory pathogenesis (Tregoning *et al.*, 2010). RSV activates multiple signaling pathways, including those involving protein kinase C (PKC), mitogen-activated protein kinase (MAPK), and nuclear factor-κB (NF-κB) (Bitko *et al.*, 1997; Bitko and Barik, 1998; Chen *et al.*, 2000; Gower *et al.*, 2001). Activation of PKC plays a role in the early stages of RSV infection (Monick *et al.*, 2001). RSV causes hypoxia-inducible factor-1α (HIF-1α) stabilization, which is important in inflammation and edema formation (Kilani *et al.*, 2004). Furthermore, proinflammatory cytokines and chemokines induced by RSV are regulated via an NF-κB pathway (Yoboua *et al.*, 2010). Therefore, we hypothesized that the PKCδ/HIF-1α/NF-κB pathway might play an important role in RSV-induced respiratory pathogenesis.

The airway epithelium is the first line of defense during respiratory virus infection (Holt *et al.*, 2008). The epithelial barrier is regulated in large part by the apicalmost intercellular junctions, referred to as tight junctions (Schneeberger *et al.*, 1992). Furthermore, tight junctions also separate the apical from the basolateral cell surface domains to establish epithelial cell polarity (Tsukita and Furuse, 1998). Tight junctions are formed by not only the integral membrane proteins claudins, occludin, tricellulin, JAMs (junctional adhesion molecules), and CAR (coxsackie and adenovirus receptor), but also many peripheral membrane proteins, including scaffold PDZ-expression proteins and cell polarity molecules (Tsukita *et al.*, 2001; Sawada *et al.*, 2003; Schneeberger and Lynch, 2004; Ikenouchi *et al.*, 2005). Moreover, it is also known that tight junctions include targets or receptors of viruses and bacteria such as claudin-1 and occludin as coreceptors of hepatitis C virus (HCV), JAM as a reovirus receptor, CAR, and some claudins as *Clostridium perfringens* enterotoxin receptors (Guttman and Finlay, 2009).

We previously reported that, in human nasal epithelial cells (HNECs) in vivo and in vitro, occludin, JAM-A, ZO-1, ZO-2, claudin-1, -4, -7, -8, -12, -13, -14, and tricellulin were detected together with well-developed tight junction strands (Takano *et al.*, 2005; Kurose *et al.*, 2007; Ohkuni *et al.*, 2009). Furthermore, the human telomerase reverse transcriptase (hTERT)-transfected HNECs with an extended life span that we previously established can be used as an indispensable and stable model for studying the regulation of tight junction proteins in human nasal epithelium (Kuruse *et al.*, 2007; Ohkuni *et al.*, 2009; Kamekura *et al.*, 2010; Ogasawara *et al.*, 2010). In TERT-transfected HNECs, treatment with transforming growth factor-β1 (TGF-β1) markedly induces claudin-4 expression (Kurose *et al.*, 2007). It is possible that tight junctions in HNECs may be useful new molecular targets for defense against respiratory virus infection.

In this study, to investigate the detailed mechanisms of replication and budding of RSV in HNECs and the epithelial cell responses, including production of proinflammatory cytokines and induction of tight junctions, we established an RSV-infected model in HNECs using hTERT-transfected cells, and examined the expression of RSV/G and F proteins and virus filaments. We first found that the expression and function of tight junction molecules were markedly induced together with production of proinflammatory cytokines in HNECs after RSV infection, and the induction of tight junction molecules contributed to budding of RSV. Furthermore, the replication and budding of RSV and the epithelial cell responses in HNECs were regulated via a PKCδ/HIF-1α/NF-κB pathway. Our data provide new insights into the signaling mechanisms that contribute to RSV-induced respiratory pathogenesis.

RESULTS

RSV infects HNECs in vitro

We quantified the susceptibility of HNECs in vitro to RSV infection by using hTERT-transfected HNECs. When the HNECs were infected with RSV at multiplicity of infection (MOI) 1, the mRNA and protein of RSV/G protein were markedly increased from 24 h (Figure 1, A and B). At 24 h after infection by RSV, the expression of RSV/G and F proteins was detected in most cells by immunocytochemistry using specific antibodies (Figure 1C). In an enzyme-linked immunosorbent assay (ELISA) of the medium, the levels of interleukin 8 (IL-8) and tumor necrosis factor-α (TNF-α) were significantly increased in the live virus group compared with the noninfected controls and the group with UV-inactivated RSV (Figure 1D).

During RSV infection, it is thought that there is a close physical interaction between the filamentous actin and the virus, which is indicated by both the virus filaments and inclusion bodies (Jeffree *et al.*, 2007). In the RSV-infected HNECs, many virus filaments were observed on the cell surface by scanning electron microscopy (SEM), and inclusion bodies were also detected at submembranes by transmission electron microscopy (TEM), but they were not detected in the control (Figure 1E).

To determine whether RSV infected from the apical or basolateral surfaces of HNECs, the cells were infected with RSV from apical or basolateral regions by using double chamber dishes. In Western blots, the RSV/G protein was detected only from the apical region (Figure 1F) and in immunocytochemistry, the expression of RSV/G from the apical group was greater than that from the basolateral group (Figure 1G). Thus HNECs were more susceptible to RSV infection from the apical surface than from the basolateral surface.

Gene expression changes in HNECs infected with RSV

We performed GeneChip analysis of HNECs infected with RSV, and selected gene probes that were up-regulated more than twofold compared with the controls (Table 1). In HNECs infected with RSV, up-regulation of IL-8 and TNF-α was confirmed together with a marked increase of the pattern recognition receptors RIG-I and MDA5. More interestingly, up-regulation of tight junction molecules claudin-2, -4, -7, -9, -14, and -19, occludin, ZO-2, cingulin, and MAGI-1 was observed in HNECs infected with RSV.

RSV infection induces tight junction protein claudin-4 in HNECs via a PKCδ/NF-κB signaling pathway

To confirm the up-regulation of tight junction proteins in HNECs infected with RSV, Western blotting, reverse transcription–PCR (RT–PCR), real-time PCR, and immunocytochemistry were performed. In Western blotting, the proteins of claudin-4 and occludin were increased gradually in a time-dependent manner after RSV infection (Figure 2A). In RT–PCR and real-time PCR, the mRNAs of claudin-4 and occludin were increased from 24 h after RSV infection, whereas no changes were observed in the non-infected control and the group with UV-inactivated RSV (Figure 2, B and C; Supplemental Figure 1). In immunocytochemistry at 24 h after

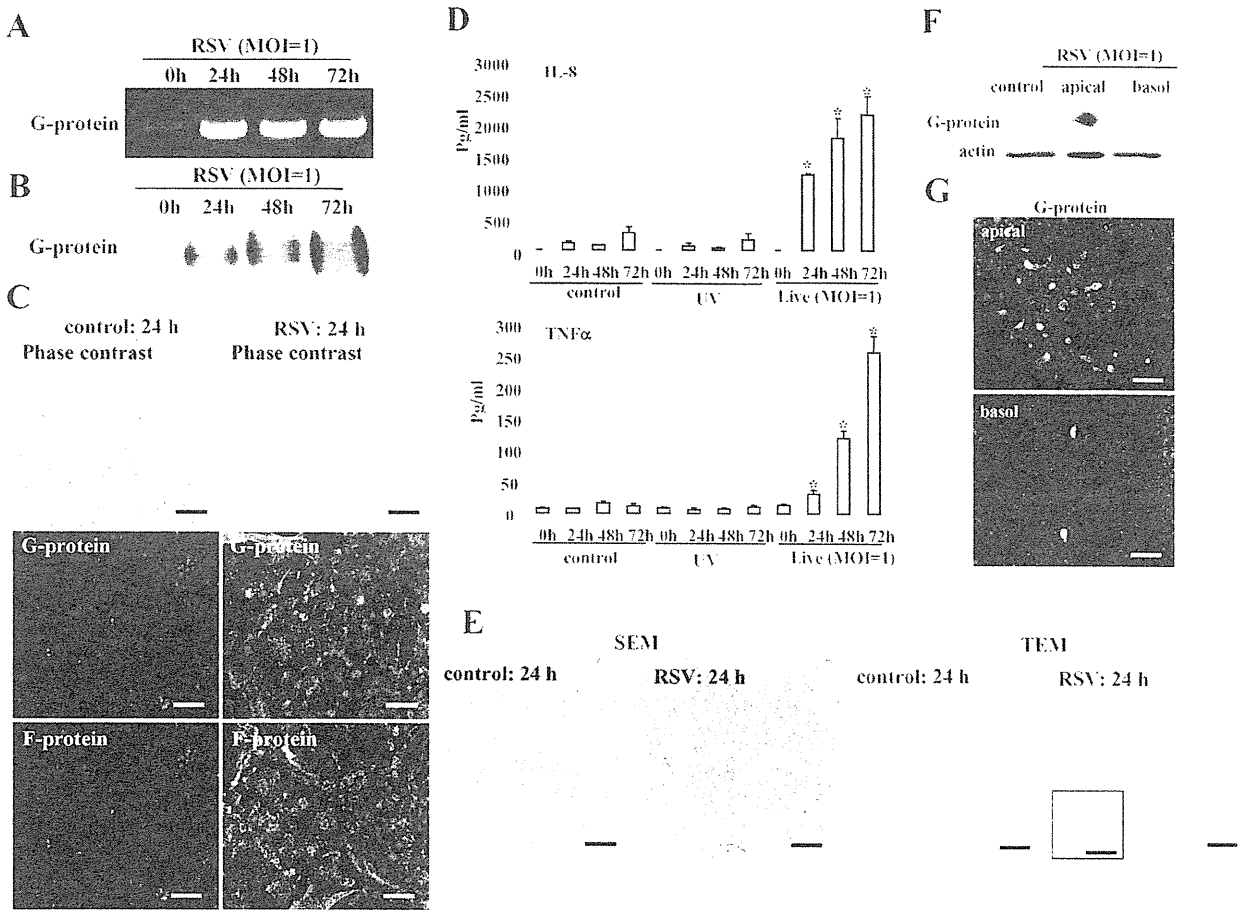

FIGURE 1: RSV-infected HNECs. RT–PCR (A) and Western blot (B) for RSV/G protein in HNECs infected with RSV at an MOI of 1. (C) Phase contrast and immunostaining for RSV/G and F proteins in HNECs at 24 h after infection with RSV at an MOI of 1. Black bar: 40 μM; white bar: 20 μM. (D) ELISA for IL-8 and TNF-α from HNECs infected with RSV at an MOI of 1 or with UV-treated RSV. UV: RSV was inactivated by exposing the virus to UV light at 1 J. Data are means ± *SEM*, *$p < 0.01$ compared with 0 h. (E) SEM image and TEM image of HNECs at 24 h after infection with RSV at an MOI of 1. SEM bars: 400 nm; TEM bars: 1 μm. Inset image: 100 nm. Western blot (F) and immunostaining (G) for RSV/G protein in HNECs infected with RSV at an MOI of 1 from apical or basolateral regions by using double-chamber dishes. Bars: 40 μM.

RSV infection, claudin-4 and occludin were increased at the membranes of HNECs, compared with the control (Figure 3).

In the control HNECs in vitro, claudin-1 and -7, ZO-1, JAM-A, and E-cadherin were also detected by Western blotting and immunocytochemistry (Kurose *et al.*, 2007). In Western blotting, only claudin-1 was decreased at 72 h after RSV infection, whereas no change of claudin-7, ZO-1, JAM-A, or E-cadherin (Supplemental Figure 2) was observed. In immunocytochemistry at 24 h after RSV infection, ZO-1, JAM-A, and E-cadherin were increased at the membranes compared with the control (Supplemental Figure 3).

To investigate which signaling pathways were associated with induction of claudin-4 by RSV infection, HNECs were pretreated with MAPK inhibitor PD98059, p38 MAPK inhibitor SB203580, phosphoinositide 3-kinase (PI3K) inhibitor LY294002, pan-PKC inhibitor GF109203X, c-Jun N-terminal kinase (JNK) inhibitor SP600125, and NF-κB inhibitor IMD-0354 at 30 min before RSV infection. In Western blotting, the up-regulation of claudin-4 after RSV infection was inhibited by pan-PKC inhibitor GF109203X and NF-κB inhibitor IMD-0354 (Figure 2D).

As the up-regulation of claudin-4 after RSV infection was inhibited by the pan-PKC inhibitor, we investigated the effects of PKC isoforms. When HNECs were pretreated with PKCα inhibitor Gö6976, PKCδ inhibitor rottlerin, PKCθ inhibitor myristoylated PKCθ pseudosubstrate peptide inhibitor, or PKCε inhibitor PKCε translocation inhibitor peptide 30 min before RSV infection, PKCδ inhibitor rottlerin prevented up-regulation of claudin-4 at the same level as pan-PKC inhibitor GF109203X (Figure 2E).

PKCδ inhibitor and NF-κB inhibitor prevent replication of RSV, formation of virus filaments, and production of proinflammatory cytokines in HNECs after RSV infection

We investigated whether the PKCδ inhibitor and NF-κB inhibitor that prevented up-regulation of claudin-4 in HNECs after RSV infection affected replication of RSV, formation of virus filaments, and expression of proinflammatory cytokines.

In Western blotting and real-time PCR, the up-regulation of claudin-4 after RSV infection was inhibited by pan-PKC inhibitor GF109203X, PKCδ inhibitor rottlerin, and NF-κB inhibitor IMD-0354 (Figure 4, A and B). In Western blots, the expression of RSV/G protein, which indicated the replication of RSV, was inhibited by the PKCδ inhibitor and NF-κB inhibitor (Figure 4A). In the ELISA, the production of IL-8 and TNF-α from HNECs after RSV infection was

Gene name	ID	Gene Bank ID	Fold change (>2.0)
CLDN2	H200002539	NM_020384	2.9
CLDN4	H300004950	NM_001305	7.3
CLDN7	H200017305	NM_001307	2.3
CLDN9	H200009827	NM_020982	3.0
CLDN14	H200016568	NM_144492; NM_012130	2.8
CLDN19	H200009873	NM_148960	2.6
OCLN	opHsV0400004868	NM_002538	2.3
TJP2 (ZO-2)	H300020004	NM_002538	4.2
CGN (Cingulin)	H300009163		3.4
BAIAP1 (MAGI-1)	H300019020	NM_004742	2.2
TGFB1	opHsV0400000071	NM_002538	2.9
PRKCD (PKCδ)	H200014060	NM_212539; NM_006254	2.2
HIF-1α	H300017074	NM_181054; NM_001530	17.2
VEGFC	H200006638	NM_005429	6.3
NT5E	H200013920	NM_002526	6.9
NFKBIA	H200006833	NM_020529; NM_020529	4.1
NFKBIE	H200010505	NM_004556	6.7
NFKBIZ	H300020290	NM_031419; NM_001005474	3.9
IL8	opHsV0400000818	NM_000584	3.2
TNFA	H200015775	NM_000594	6.0
DDX58 (RIG1)	H200013521	NM_014314	37.1
IFIH1 (MDA5)	H200009565	NM_022168	25.9

TABLE 1: Gene probes that are up-regulated more than twofold to the control in RSV-infected hTERT-HNECs.

also inhibited by the PKCδ inhibitor and the NF-κB inhibitor (Figure 4C). In immunocytochemistry, up-regulation of claudin-4 and expression of RSV/G protein after RSV infection were markedly inhibited by the pan-PKC inhibitor, PKCδ inhibitor, and NF-κB inhibitor (Figure 4, D and E). Furthermore, the formation of virus filaments after RSV infection was inhibited by the pan-PKC inhibitor, PKCδ inhibitor, and NF-κB inhibitor (Figure 4F). When we investigated the cytotoxicity of the inhibitors of pan-PKC, PKCδ, and NF-κB in HNEC cells after RSV infection, cytotoxicity was not observed at the concentration of all inhibitors (Supplemental Figure 4).

RSV infection induces formation of tight junction strands and barrier function via up-regulation of claudin-4 in HNECs

To investigate whether RSV induced the formation of tight junction strands and barrier function of HNECs, freeze-fracture and transepithelial electrical resistance (TER) measurement were performed. In freeze-fracture replicas at 24 h after RSV infection, the mean number of tight junction strands was significantly increased compared with the control and well-developed networks formed by continuous lines of tight junction strands (Figure 5A). For the barrier function, TER values were significantly increased by RSV infection from apical regions of HNECs compared with the control and RSV infection from basolateral regions (Figure 5B).

PKCδ inhibitor and NF-κB inhibitor prevent budding of RSV from apical surface of HNECs

In immunocytochemistry at 24 h after RSV infection, RSV/G and /F proteins were detected at submembranes of the HNEC apical surface, whereas they were observed around the nuclei at 8 h after RSV infection (Figure 5C). When RSV/G and /F proteins were detected at submembranes of the HNEC apical surface at 24 h after RSV infection, tight junction protein ZO-1 was observed at cell borders (Figure 5C).

In SEM at 24 h after RSV infection, many small membranous substances were observed at the surfaces of HNECs together with cilia, whereas they were not detected in the control (Figure 5D). It is thought that they indicate budding of RSV, because in TEM at 24 h after RSV infection, a complex of electric, high-density particles is observed in the small membranous substances at the surface and in submembranes of HNECs (Figure 5D). Furthermore, pan-PKC inhibitor GF109203X, PKCδ inhibitor rottlerin, and NF-κB inhibitor IMD-0354 prevented the budding of RSV (Figure 5D).

RSV infection induces expression of claudin-4 but not RSV replication via production of TGF-β1 from HNECs

RSV infection induces the expression of TGF-β in epithelial A594 and PHBE cells (Gibbs *et al.*, 2009). We previously reported that treatment with TGF-β could induce the expression of claudin-4 in HNECs (Kurose *et al.*, 2007). Furthermore, in the present study, when we performed GeneChip analysis of HNECs infected with RSV, up-regulation of TGF-β1 and TGF-β receptor II was observed together with an increase of claudin-4 (Table 2).

We investigated whether up-regulation of claudin-4 in HNECs after RSV infection was caused via TGF-β signaling. In RT–PCR and real-time PCR after RSV infection, mRNAs of RSV/G

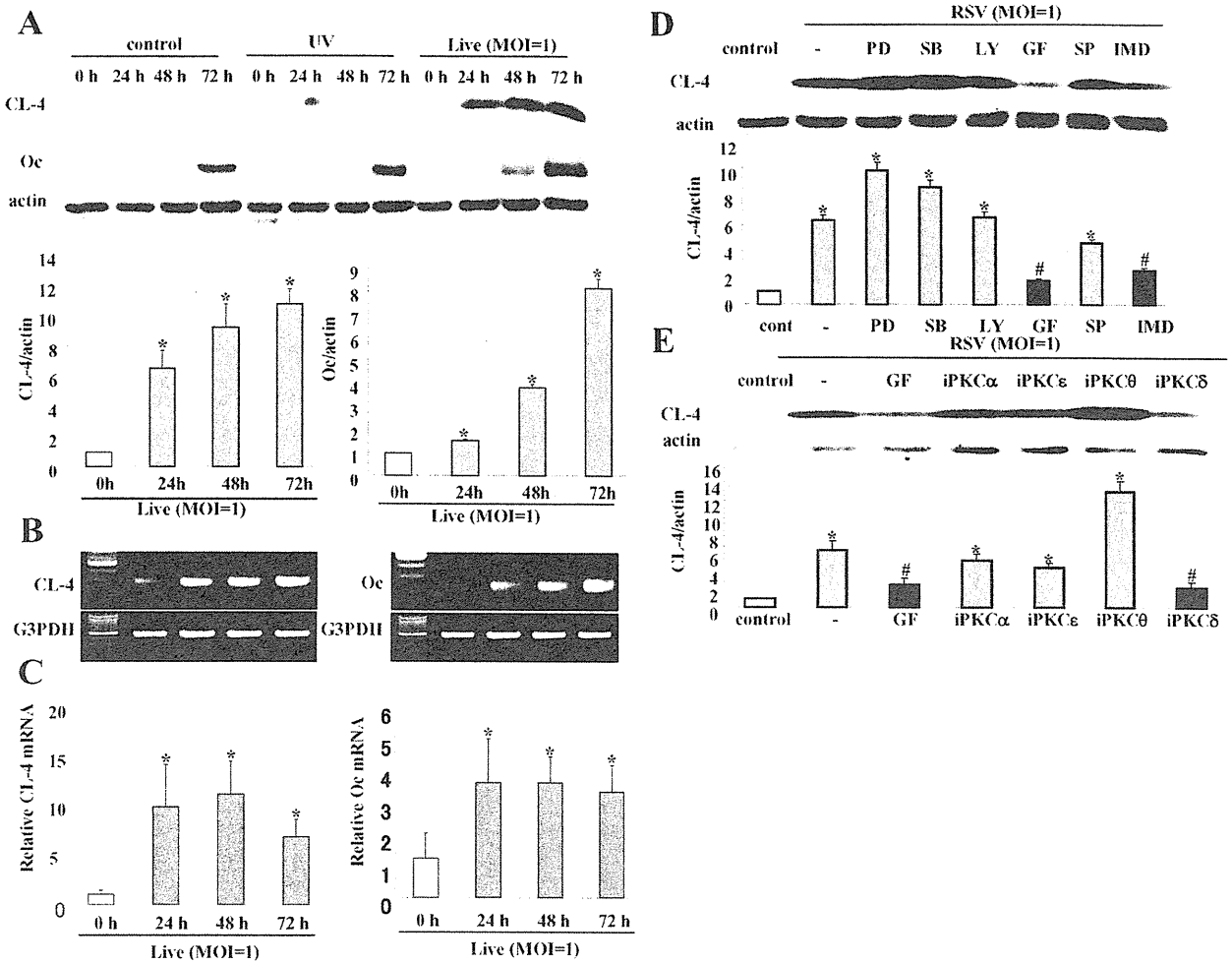

FIGURE 2: Induction of claudin-4 and occludin in HNECs infected with RSV. (A) Western blot for claudin-4 and occludin in HNECs infected with RSV at an MOI of 1 or with UV-treated RSV. The corresponding expression levels of (A) are shown as bar graphs. Data are means ± *SEM*, *p < 0.01 compared with 0 h. RT–PCR (B) and real-time PCR (C) for claudin-4 and occludin in HNECs infected with RSV at an MOI of 1. Data are means ± *SEM*, *p < 0.01 compared with 0 h. (D) Western blot for claudin-4 in HNECs pretreated with inhibitors of signaling pathways 30 min before infection with RSV at an MOI of 1 for 24 h. The corresponding expression levels of (D) are shown as bar graphs. Data are means ± *SEM*, *p < 0.01 compared with control, #p < 0.01 compared with RSV. PD: MAPK inhibitor PD98059; SB: p38 MAPK inhibitor SB203580; LY: PI3K inhibitor LY294002; GF: pan-PKC inhibitor GF109203X; SP: JNK inhibitor SP600125; IMD: NF-κB inhibitor IMD-0354. (E) Western blot for claudin-4 in HNECs pretreated with inhibitors of PKC isoforms 30 min before infection with RSV at an MOI of 1 for 24 h. GF: pan-PKC inhibitor GF109203X; iPKCα: PKCα inhibitor Gö6976; iPKCδ: PKCδ inhibitor rottlerin; i PKCθ: PKCθ inhibitor myristoylated PKCθ pseudosubstrate peptide inhibitor; iPKCε: PKCε inhibitor PKCε translocation inhibitor. The corresponding expression levels of (E) are shown as bar graphs. Data are means ± *SEM*, *p < 0.01 compared with control, #p < 0.01 compared with RSV.

protein, TGF-β1, and claudin-4 were significantly increased from 3 h, 12 h, and 24 h, respectively (Figure 6, A–C). The up-regulation of mRNAs of TGF-β1 and claudn-4 in HNECs after RSV infection was maintained from 24 h until 72 h, whereas no changes were observed in the non-infected control and the group with UV-inactivated RSV (Figure 6, D–F; Supplemental Figure 1). In Western blotting and real-time PCR, up-regulation of claudin-4 after RSV infection was inhibited by TGF-β receptor I kinase inhibitor (iTGF-βR; Figure 6, G and H), but expression of RSV/G protein, which indicated replication of RSV, was not inhibited by the iTGF-βR (Figure 6, G and H). In immunocytochemistry, the iTGF-βR prevented up-regulation of claudin-4 at the membranes but not expression of RSV/G protein after RSV infection (Figure 6I).

Possible regulation of claudin-4 in HNECs after RSV infection via a TGF-β1/PKCδ/HIF-1α/NF-κB signaling pathway

In GeneChip analysis of HNECs infected with RSV, up-regulation of PKCδ, HIF-1α, HIF-1α–associated genes VEGF and NT5, and NF-κB was observed (Table 1). Furthermore, in Western blotting, phospho-PKCδ, HIF-1α, and phospho-NF-κB were increased together with induction of claudin-4 after RSV infection (Figure 7A).

For the mechanisms of the up-regulation of claudin-4 in HNECs after RSV infection, we hypothesized the possible regulation of claudin-4 via a TGF-β1/PKCδ/HIF-1α/NF-κB signaling pathway and confirmed it by using treatment with TGF-β1 and under hypoxia (2% O_2).

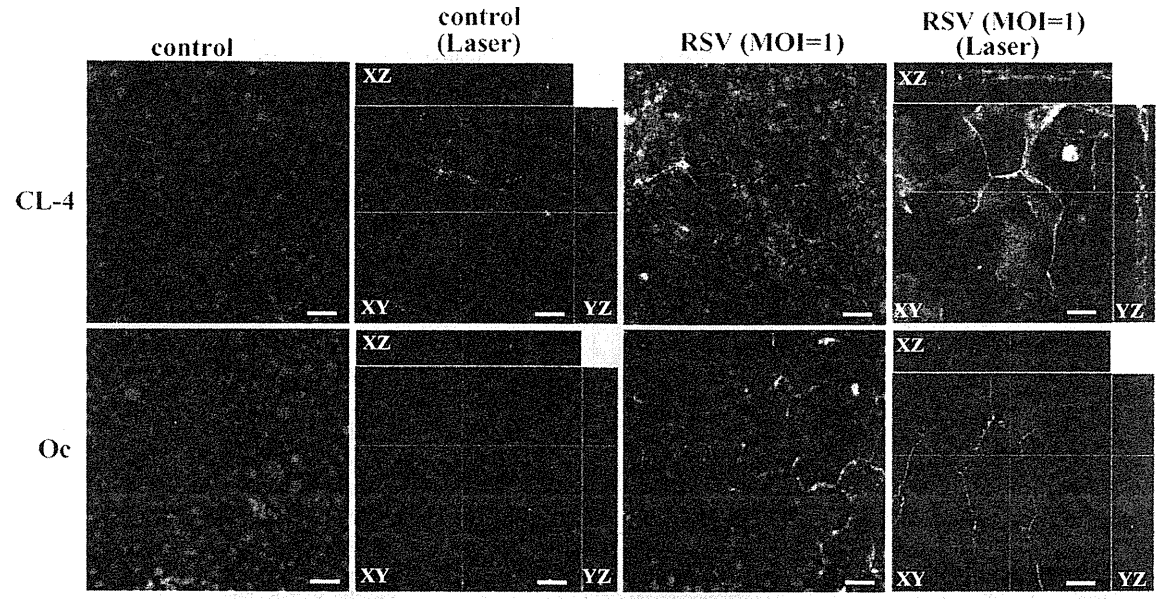

FIGURE 3: Images of inverted microscope and confocal laser scanning microscope using immunostaining for claudin-4 and occludin in HNECs 24 h after infection with RSV at an MOI of 1.

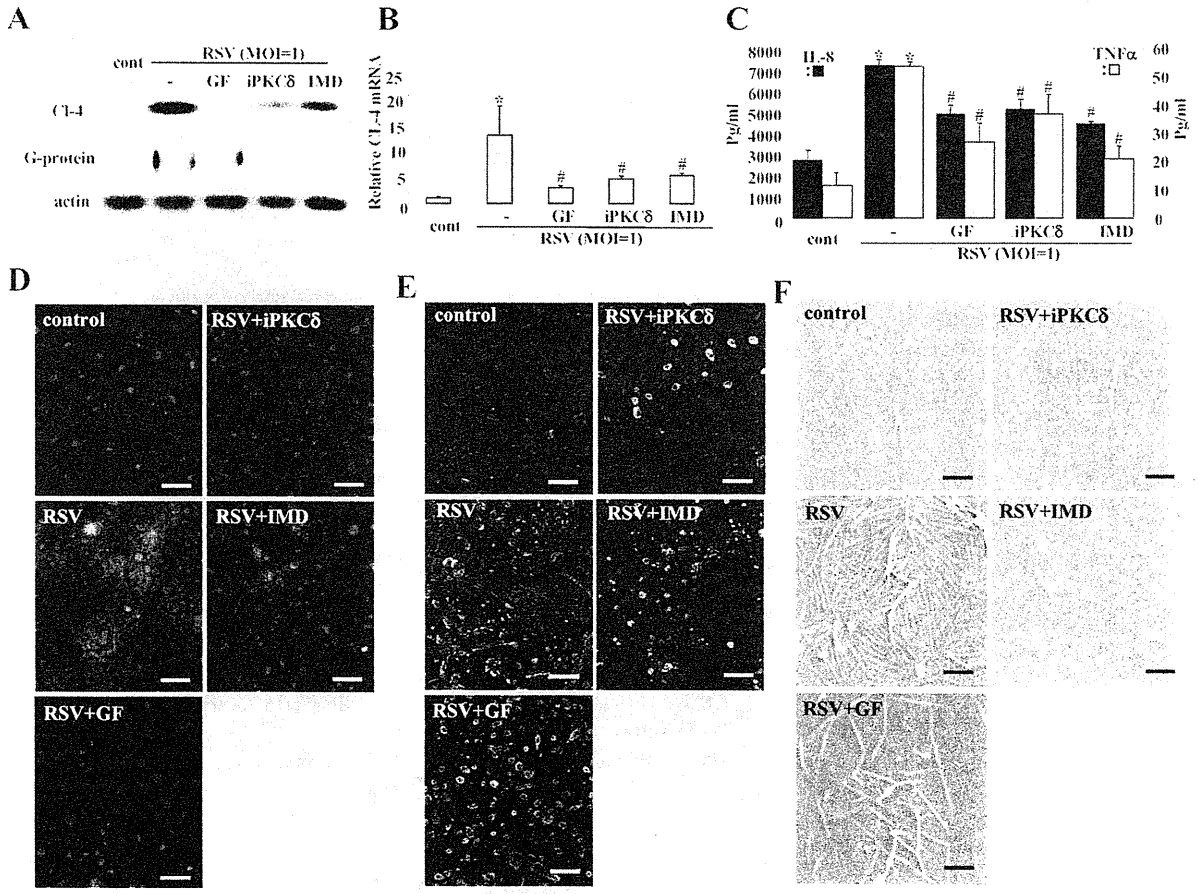

FIGURE 4: Inhibitors of pan-PKC, PKCδ, and NF-κB prevent replication of RSV and the epithelial cell responses in HNECs infected with RSV. Western blot (A) for claudin-4 and RSV/G protein, real-time PCR (B) for claudin-4, ELISA (C) for IL-8 and TNF-α, immunostaining for claudin-4 (D) and RSV/G protein (E), and SEM images (F) of HNECs pretreated with inhibitors of pan-PKC, PKCδ, and NF-κB 30 min before infection with RSV at an MOI of 1 for 24 h. GF: pan-PKC inhibitor GF109203X; iPKCδ: PKCδ inhibitor rottlerin; IMD: NF-κB inhibitor IMD-0354. Data are means ± *SEM*, *$p < 0.01$ compared with control, #$p < 0.01$ compared with RSV. Bars of D and E: 40 μm, Bars of F: 1 μm.

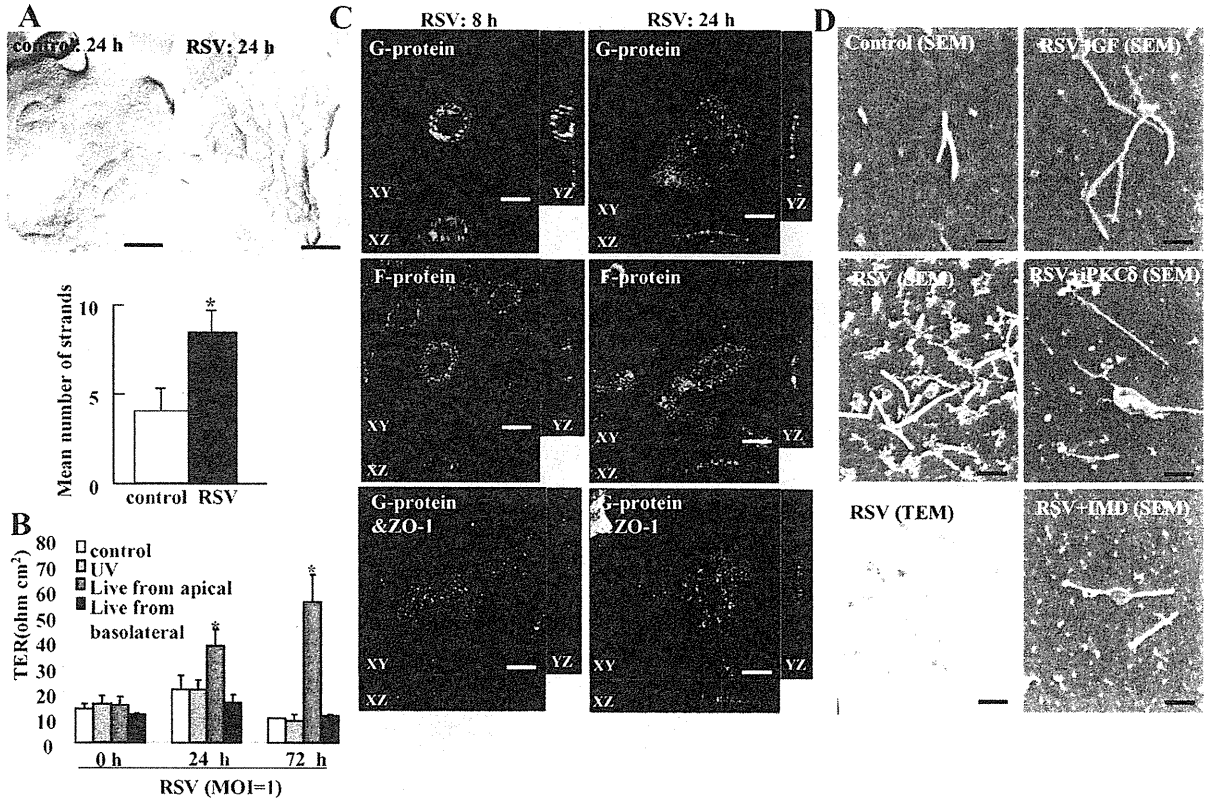

FIGURE 5: Structures and barrier function of tight junctions in HNECs infected with RSV. (A) Freeze-fracture replica of HNECs 24 h after infection with RSV at an MOI of 1. Bar: 200 nm. Morphometric analysis of tight junction strands of A is shown as a bar graph. *$p < 0.01$ compared with control. (B) Barrier function measured as TER in HNECs infected with RSV at an MOI of 1 from apical or basolateral regions by using double-chamber dishes or with UV-treated RSV. UV: RSV was inactivated by exposing the virus to UV light at 1 J. Data are means ± *SEM*, *$p < 0.01$ compared with 0 h. (C) Immunostaining for RSV/G and F proteins and ZO-1 in HNECs at 8 h and 24 h after infection with RSV at an MOI of 1. Bars: 10 μm. (D) SEM images and TEM image of HNECs pretreated with inhibitors of pan-PKC, PKCδ, and NF-κB at 30 min before infection with RSV at an MOI of 1 for 24 h. GF: pan-PKC inhibitor GF109203X; iPKCδ: PKCδ inhibitor rottlerin; IMD: NF-κB inhibitor IMD-0354. Bars of SEM: 1 μm; Bar of TEM: 400 nm.

When HNECs were treated with 0.1–10 ng/ml TGF-β1 for 24 h, up-regulation of claudin-4, phospho-PKCδ, HIF-1α, and phospho-NF-κB was increased from 0.1, 0.1, 0.1, and 1 ng/ml, respectively, in Western blotting (Figure 7B). In RT–PCR, HIF-1α mRNA was increased from 0.1 ng/ml TGF-β1 (Supplemental Figure 5). In Western blotting, up-regulation of claudin-4 after treatment with 10 ng/ml TGF-β was inhibited by iTGF-βR (Figure 7C).

When HNECs were incubated in a 5% CO_2/2% O_2 incubator balanced by nitrogen for 24 h, claudin-4, phospho-PKCδ, HIF-1α, and phospho-NF-κB were increased from 1, 2, 2, and 1 h after treatment with hypoxia, respectively, in Western blotting (Figure 7D). In RT–PCR, HIF-1α mRNA was increased from 2 h (Supplemental Figure 5).

Possible regulation of claudin-4 in HNECs after RSV infection and replication of RSV via a HIF-1α signaling pathway

To investigate whether HIF-1α directly affected claudin-4 expression and replication of RSV after the infection, HNECs were pretreated with three siRNAs of HIF-1α before RSV infection. Two siRNAs of HIF-1α slightly prevented up-regulation of claudin-4 and expression of RSV/G protein at 24 h after RSV infection in Western blotting (Figure 8A).

DISCUSSION

In the present study, we established an RSV-infected model in HNECs using hTERT-transfected cells and to our knowledge first demonstrated that the replication and budding of RSV and the epithelial cell responses in HNECs were regulated via a PKCδ/HIF-1α/NF-κB pathway.

In the polarized cells of respiratory tract epithelium, RSV enters through the apical surface, and the assembly and budding of the virus occur at the apical membrane (Roberts *et al.*, 1995; Zhang *et al.*, 2002; Wright *et al.*, 2005). In hTERT-transfected HNECs after RSV infection, RSV/G and F proteins were detected in most cells together with production of proinflammatory cytokines IL-8 and TNF-α. Furthermore, RSV entered through the apical surface of the HNEC, and the assembly and budding of the virus, indicated as virus filaments and many small membranous substances, also occurred at the apical membrane or submembrane. These results suggested that hTERT-transfected HNECs might function as an RSV-infected model for HNECs to investigate the regulation of replication and budding of the virus and the epithelial cell responses.

Some claudins are degraded during West Nile virus infection (Medigeshi *et al.*, 2009). In polarized airway epithelial cells infected with rhinoviruses, TER is decreased together with the loss of ZO-1 (Sajjan *et al.*, 2008). Infection with mouse adenovirus type 1 results in reduced expression and cell surface localization of tight junction

Antibody	Type	Dilution		Source
		IC	WB	
Claudin-1	pAb		1:1000	Zymed Laboratories (San Francisco, CA)
Claudin-4	pAb	1:100	1:1000	Zymed Laboratories
Claudin-7	pAb		1:1000	Zymed Laboratories
Occludin	pAb	1:100	1:1000	Zymed Laboratories
JAM-A	pAb	1:100	1:1000	Zymed Laboratories
ZO-1	pAb	1:100	1:1000	Zymed Laboratories
E-cadherin	mAb (36/E-cadherin)	1:200	1:1000	BD Biosciences (San Jose, CA)
RSV/G and /F proteins	mAb	1:100	1:4000	Tsutsumi *et al.*, 1989
HIF-1α	mAb		1:1000	Novus Biologicals (Littleton, CO)
Phospho-PKCδ	pAb		1:1000	Cell Signaling Technology (Danvers, MA)
PKCδ	mAb		1:1000	BD PharMingen (San Diego, CA)
Phospho-pan-PKC	pAb		1:1000	Cell Signaling Technology
Pan-PKC	pAb		1:1000	Santa Cruz Biotechnology (Santa Cruz, CA)
Phospho-NF-κB	pAb		1:1000	Cell Signaling Technology
NF-κB	pAb		1:1000	Cell Signaling Technology
Actin	pAb		1:1000	Sigma-Aldrich

pAb, rabbit polyclonal antibody; mAb, mouse mAb.

TABLE 2: Antibodies.

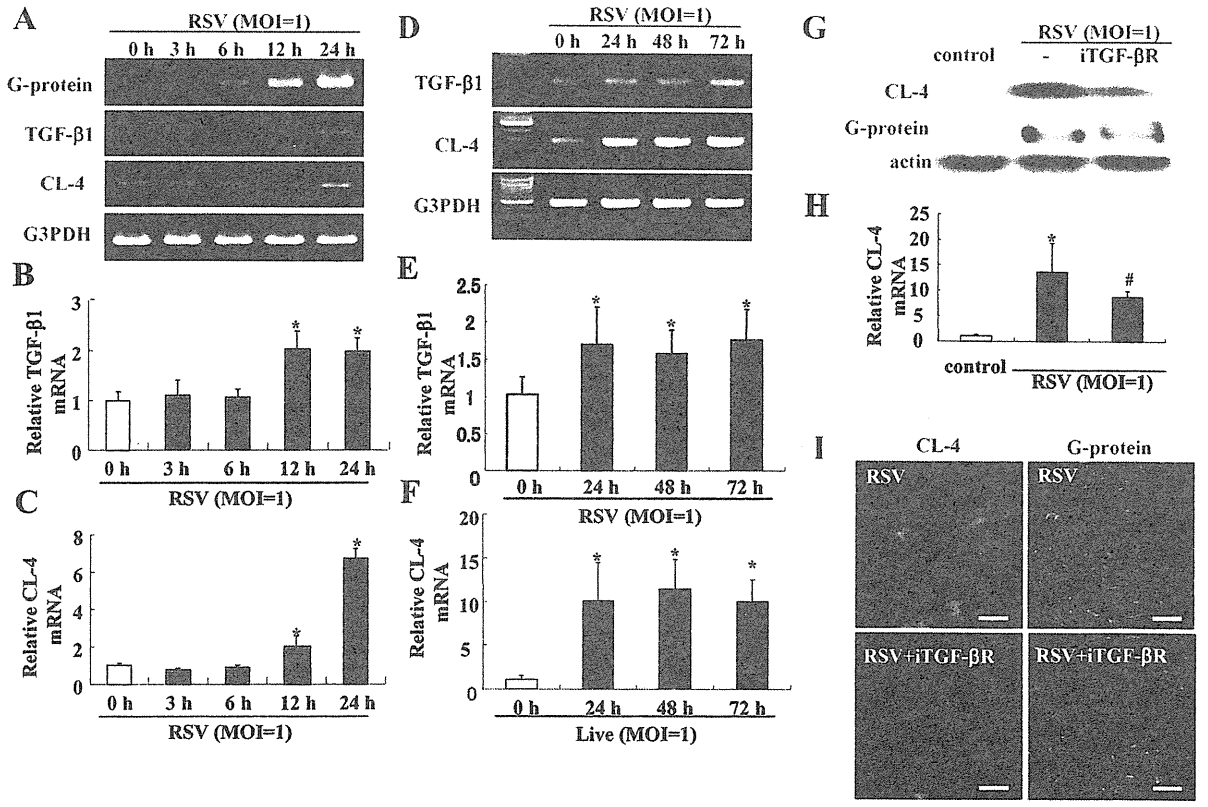

FIGURE 6: Induction of TGF-β1 in HNECs infected with RSV. RT–PCR (A and D) and real-time PCR (B, C, E, and F) for RSV/G protein, TGF-β1, and claudin-4 in HNECs infected with RSV at an MOI of 1. Data are means ± *SEM*, *$p < 0.01$, compared with 0 h. Western blot (G) and real-time PCR (H) for claudin-4, and immunostaining (I) for claudin-4 and RSV/G protein in HNECs pretreated with iTGF-βR 30 min before infection with RSV at an MOI of 1 for 24 h. Data are means ± *SEM*, *$p < 0.01$ compared with control, #$p < 0.01$ compared with RSV. Bars: 40 μm.

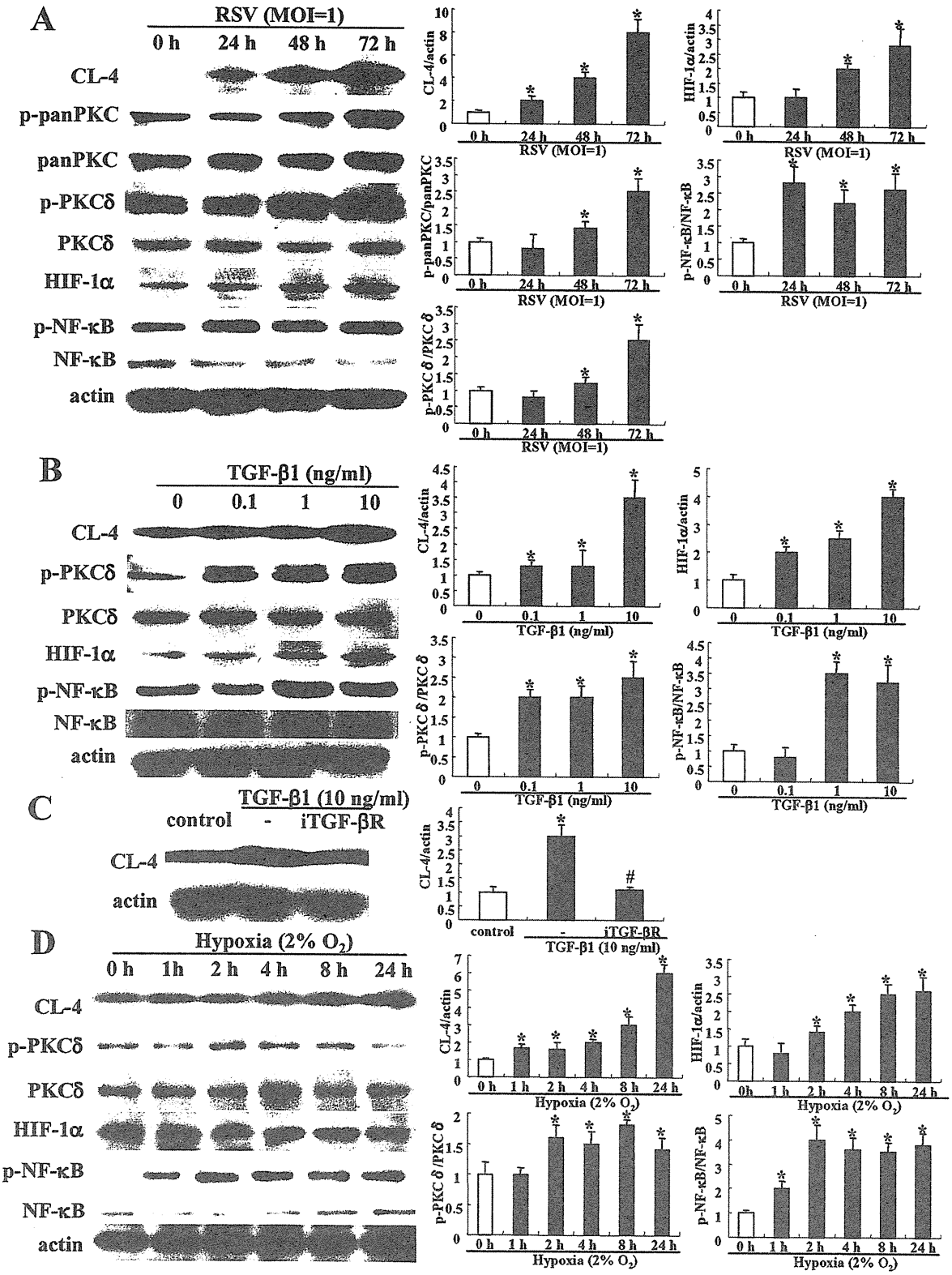

FIGURE 7: Induction of claudin-4 in HNECs via a TGF-β/PKCδ/HIF-1α/NK-κB pathway. (A) Western blot for claudin-4, phospho-pan-PKC, phospho-PKCδ, HIF-1α, and phospho-NK-κB in HNECs infected with RSV at an MOI of 1. Western blot (B) for claudin-4, phospho-PKCδ, HIF-1α ,and phospho-NK-κB in HNECs at 24 h after treatment with 0.1–10 ng/ml TGF-β1. (C) Western blot for claudin-4 in HNECs pretreated with iTGF-βR 30 min before treatment with 10 ng/ml TGF-β1. Western blot (D) for claudin-4, phospho-PKCδ, and phospho-NK-κB in HNECs 24 h after treatment with hypoxia. The corresponding expression levels of (A–D) are shown as bar graphs. Data are means ± *SEM*. *$p < 0.01$ compared with control, #$p < 0.01$ compared with RSV.

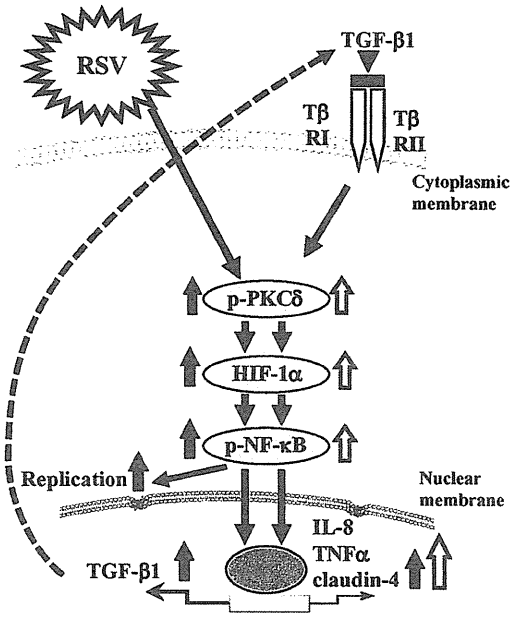

FIGURE 8: Overview of signal transduction events in HNECs infected with RSV.

proteins along with loss of barrier properties (Gralinski *et al.*, 2009). The effects of RSV infection on tight junctions of upper airway HNECs remain known, however.

RSV infection alters the expression of adhesion molecules intercellular adhesion molecule 1 and E-cadherin in A549 cells (Wang *et al.*, 2000). When we performed GeneChip analysis of HNECs infected with RSV compared with the control, we found dramatic up-regulation of tight junction molecules claudin-2, -4, -7, -9, -14, and -19, occludin, ZO-2, cingulin, and MAGI-1, together with up-regulation of proinflammatory cytokines IL-8 and TNF-α, as well as viral double-strand-RNA–induced pattern recognition receptors RIG-I and MAD5. In HNECs infected with live RSV, but not UV-treated RSV, up-regulation of claudin-4 and occludin was confirmed at the levels of protein and mRNA together with up-regulation of the tight junctional barrier function, whereas claudin-1 was decreased at 72 h after RSV infection. In immunocytochemistry at 24 h after RSV infection, not only claudin-4 and occludin but also ZO-1, JAM-A, and E-cadherin were increased at the membranes together with localization of RSV/G and /F proteins at submembranes of the apical surface. These results suggested that the tight junction molecules induced after RSV infection, which also play a crucial role in epithelial cell polarity, might contribute to the budding of the virus from the HNEC apical surface.

It is known that RSV activates multiple signaling pathways, including those involving PKC, MAPK, and NF-κB (Bitko *et al.*, 1997; Bitko and Barik, 1998; Chen *et al.*, 2000; Gower *et al.*, 2001). Activation of PKC plays a role in the early stages of RSV infection (Monick *et al.*, 2001). Previous studies have shown that PKC activation plays a role in the early stages of RSV infection (Sieczkarski *et al.*, 2003) and RSV activates PKCδ at early time points after infection by the virus (Monick *et al.*, 2001). RSV causes HIF-1α stabilization, which is important in inflammation and edema formation (Kilani *et al.*, 2004). Furthermore, proinflammatory cytokines and chemokines induced by RSV are regulated via an NF-κB pathway (Yoboua *et al.*, 2010). In the present study, in HNECs after RSV infection, up-regulation of phospho-PKCδ, HIF-1α, and phospho-NF-κB was observed by Western blotting. Upregulation of claudin-4 in HNECs after RSV infection was prevented by inhibitors of PKCδ and NF-κB. The inhibitors of PKCδ and NF-κB also prevented expression of RSV/G protein, the presence of virus filaments and small membranous substances at the apical membrane or submembrane, and production of proinflammatory cytokines after RSV infection. These results suggest that a PKCδ/HIF-1α/NF-κB pathway plays an important role in the replication and budding of RSV and the epithelial cell responses in HNECs.

RSV infection induces the expression of TGF-β in epithelial A594 and PHBE cells and causes cell-cycle arrest of lung epithelial cells through a TGF-β autocrine pathway (Gibbs *et al.*, 2009). The TGF-β signaling pathway is mediated via PKCδ (Lee *et al.*, 2005). Furthermore, we previously reported that treatment with TGF-β1 could induce claudin-4 expression at the protein and mRNA levels in HNECs (Kurose *et al.*, 2007). We investigated whether TGF-β was closely associated with up-regulation of claudin-4 expression after RSV infection. In HNECs after RSV infection, an increase of TGF-β1 mRNA was observed by GeneChip analysis (Table 1). It was enhanced later than the presence of mRNA of RSV/G protein and earlier than the increase of claudin-4 mRNA, and was maintained, like claudin-4 mRNA, for a long time. iTGF-βR prevented up-regulation of claudin-4 protein but not the presence of RSV/G protein in HNECs after RSV infection. Treatment with TGF-β1 induced not only claudin-4 expression but also expression of HIF-1α, phospho-PKCδ, and phospho-NF-κB in HNECs. These findings indicated that up-regulation of claudin-4 after RSV infection was in part regulated by a TGF-β/PKCδ/HIF-1α/NF-κB pathway in a TGF-β autocrine manner.

PKCδ regulates the stability of HIF-1α under hypoxia (Lee *et al.*, 2007). HIF-1α has been identified as a key regulator of the inflammatory transcription factor NF-κB (Walmsley *et al.*, 2005). In the present study, GeneChip analysis of HNECs after RSV infection showed that expression of PKCδ, HIF-1α, and the HIF-1α-associated genes VEGF and NT5 was increased (Table 1). To investigate whether HIF-1α directly regulated expression of claudin-4 and the replication of RSV in HNECs after the virus infection, HNECs were incubated under hypoxia or treated with siRNAs of HIF-1α. In HNECs cultured under hypoxia, up-regulation of HIF-1α, claudin-4, phospho-PKCδ, and phospho-NF-κB was observed. In HNECs after RSV infection, siRNAs of HIF-1α prevented up-regulation of claudin-4 and the presence of RSV/G protein. These results suggested that HIF-1α directly regulated the replication of RSV and the epithelial cell response in HNECs.

Some tight junction molecules are also receptors of viruses. These receptors include JAM as a reovirus receptor, CAR, and claudin-1 and occludin as coreceptors of HCV (Cohen *et al.*, 2001; Campbell *et al.*, 2005; Evans *et al.*, 2007; Guttman and Finlay, 2009; Ploss *et al.*, 2009). We investigated the possibility that claudin-4 and occludin, which were induced after RSV infection, were receptors of RSV in HNECs. When HNECs were pretreated with siRNAs of claudin-4 or occludin, however, no changes of RSV/G protein, virus filaments, and many small membranous substances were observed in HNECs after RSV infection (Supplemental Figure 6, A and B). These findings indicate that claudin-4 and occludin are not receptors of RSV in HNECs and that there are other mechanisms of the budding of RSV.

In conclusion, we established an RSV-infected model in normal HNECs using hTERT-transfected cells and found that the replication and budding of RSV and the epithelial cell responses in HNECs were regulated via a PKCδ/HIF-1α/NF-κB pathway. In addition, it was thought that the PKCδ/HIF-1α/NF-κB pathway via TGF-β in an autocrine manner might also be important in the epithelial cell responses at the late stage after RSV infection (Figure 8). Inhibition of replication and budding of RSV in upper airway HNECs via these mechanisms might contribute to useful new preventive treatments for severe lower respiratory tract disease in infants and young children.

siRNA	Sense sequence	Antisense sequence
Claudin-4–siRNA1	5′-GCAACAUUGUCACCUCGCAGACCAU-3′	5′-AUGGUCUGCGAGGUGACAAUGUUGC-3′
Claudin-4–siRNA2	5′-UCCUGUUGGCCGGCCUUAUGGUGAU-3′	5′-AUCACCAUAAGGCCGGCCAACAGGA-3′
Occludin–siRNA1	5′-UGGAUGACUUCAGGCAGCCUCGUUA-3′	5′-UAACGAGGCUGCCUGAAGUCAUCCA-3′
Occludin-siRNA2	5′-GGCCUCUUGAAAGUCCACCUCCUUA-3′	5′-UAAGGAGGUGGACUUUCAAGAGGCC-3′

TABLE 3: siRNAs.

MATERIALS AND METHODS

Reagents and inhibitors

Recombinant human IL-8, TNF-α, and TGF-β1 were purchased from PeproTech EC (London, UK). A pan-PKC inhibitor (GF109203X), MAPK inhibitor (PD98059), p38 MAPK inhibitor (SB203580), PI3K inhibitor (LY294002), PKCα inhibitor (Gö6976), PKCδ inhibitor (rottlerin), PKCθ inhibitor (myristoylated PKCθ pseudosubstrate peptide inhibitor), PKCε inhibitor (PKCε translocation inhibitor peptide), and iTGF-βR were purchased from Calbiochem-Novabiochem (San Diego, CA). JNK inhibitor SP600125 and NF-κB inhibitor IMD-0354 were purchased from Sigma-Aldrich (St. Louis, MO). Alexa 488 (green)– and Alexa 594 (red)–conjugated anti–mouse and anti–rabbit immunoglobulin G (IgG) antibodies were purchased from Molecular Probes (Eugene, OR). Horseradish peroxidase–conjugated polyclonal goat anti–rabbit IgGs were purchased from Dako (Glostrup, Denmark). The enhanced chemiluminescence Western blotting system was obtained from GE Healthcare UK (Buckinghamshire, UK).

Cell culture and treatments

The cultured HNECs were derived from mucosal tissues of patients with hypertrophic rhinitis or chronic sinusitis who underwent inferior turbinectomy at Sapporo Medical University, the Sapporo Hospital of Hokkaido Railway Company, or the KKR Sapporo Medical Center Tonan Hospital. Informed consent was obtained from all patients, and this study was approved by the ethics committees of the above institutions.

The methods for primary culture of HNECs were as reported previously (Koizumi *et al.*, 2008). Some primary cultured HNECs were transfected with the catalytic component of telomerase, the human catalytic subunit of the hTERT gene, as described previously (Kurose *et al.*, 2007; Kamekura *et al.*, 2009; Ohukuni *et al.*, 2009, Ogasawara *et al.*, 2010). The cells were plated on 35-mm or 60-mm culture dishes (Corning Glass Works, Corning, NY), which were coated with rat tail collagen (500 μg of dried tendon/ml 0.1% acetic acid). The cells were cultured in serum-free bronchial epithelial cell basal medium (Lonza Walkersville, Walkersville, MD) supplemented with bovine pituitary extract (1% vol/vol), 5 μg/ml insulin, 0.5 μg/ml hydrocortisone, 50 μg/ml gentamicin, 50 μg/ml amphotericin B, 0.1 ng/ml retinoic acid, 10 μg/ml transferrin, 6.5 μg/ml triiodothyronine, 0.5 μg/ml epinephrine, 0.5 ng/ml epidermal growth factor (Lonza Walkersville), 100 U/ml penicillin, and 100 μg/ml streptomycin (Sigma-Aldrich) and were incubated in a humidified, 5% CO_2/95% air incubator at 37°C. In this experiment, second and third passaged cells were used.

Human RSV was grown in the human laryngeal carcinoma cell line HEp-2. For infection, HNECs at 80% confluence were adsorbed at an RSV MOI of 1 for 60 min at 37°C. After adsorption, the viral solutions were removed and the cells were rinsed twice with growth medium and incubated. The virus titers in the supernatant were determined by a plaque-forming assay with HEp-2 cells. Expression of RSV mRNA was confirmed by RT–PCR.

Some cells were treated with 0.1–10 μg/ml TGF-β1 or incubated in a 2% CO_2/2% O_2 incubator balanced by nitrogen. They were pretreated with 10 μM PD98059, 10 μM SB203580, 10 μM LY294002, 10 μM GF109203X, 10 μM SP600125, 0.1 μM IMD-0354, 5 μM PKCα inhibitor, 10 μM PKCε inhibitor, 5 μM PKCθ inhibitor, 5 μM PKCδ inhibitor, and iTGF-βR at 30 min before RSV infection or treatment with 10 ng/ml TGF-β1.

siRNA experiment

For knockdown of human HIF-1α, human claudin-4, and human occludin, Stealth Select RNAi against the genes was synthesized by Invitrogen (Carlsbad, CA). The sequences for the sense and antisense strands are shown in Table 3. The hTERT-transfected HNECs at 24 h after plating were transfected with 100 nM siRNA using Lipofectamine RNAiMAX Reagent (Invitrogen). At 48 h after transfection, the cells were infected with RSV for 24 h.

RNA isolation, RT–PCR, and real-time PCR analysis

Total RNA was extracted and purified using TRIzol (Invitrogen). One microgram of total RNA was reverse-transcribed into cDNA using a mixture of oligo(dT) and Superscript II reverse transcriptase, according to the manufacturer's recommendations (Invitrogen). Synthesis of each cDNA was performed in a total volume of 20 μl for 50 min at 42°C and terminated by incubation for 15 min at 70°C. PCR was performed in a 20 μl total mixture containing 100 pM primer pairs, 1.0 μl of the 20-μl total RT product, PCR buffer, deoxyribonucleotides, and Taq DNA polymerase, according to the manufacturer's recommendations (Takara, Kyoto, Japan). Amplifications were for 25–35 cycles, depending on the PCR primer pair, with cycle times of 15 s at 96°C, 30 s at 55°C, and 60 s at 72°C. Final elongation time was 7 min at 72°C. Seven microliters of the total 20 μl of PCR product was analyzed by 1% agarose gel electrophoresis with ethidium bromide staining and was standardized using a GeneRuler TM 100BP DNA ladder (Fermentas, Ontario, Canada). To provide a quantitative control for reaction efficiency, PCRs were performed with primers coding for the housekeeping gene glyceraldehyde-3-phosphate dehydrogenase (G3PDH). Primers used to detect G3PDH and claudin-4, occludin, RSV G protein, TGF-β1, and HIF-1α are indicated in Table 4.

Real-time PCR detection was performed using a TaqMan Gene Expression Assay kit with a StepOnePlus real-time PCR system (Applied Biosystems, Foster City, CA). The amount of 18S rRNA (Hs99999901) mRNA in each sample was used to standardize the quantities of the following mRNAs: claudin-4 (Hs00533616), occludin (Hs00170162), TGF-β1 (Hs00998133), and HIF-1α (Hs00936366). The relative mRNA expression levels between the control and treated samples were calculated by the difference of the threshold cycle (comparative C_T [$\Delta\Delta C_T$] method) and presented as the average of triplicate experiments with a 95% confidence interval.

ELISA

The concentrations of human IL-8 and TNF-α in cell culture supernatants of hTERT-transfected HNECs at 24–72 h after treatment with RSV were measured using ELISA kits for human IL-8 and TNF-α (R&D Systems, Minneapolis, MN), according to the manufacturer's instructions.

Gene	Forward primer	Reverse primer	Product size (base pairs)
Claudin-4	AGCCTTCCAGGTCCTCAACT	AGCAGCGAGTCGTACACCTT	249
Occludin	TCAGGGAATATCCACCTATCACTTCAG	CATCAGCAGCAGCCATGTACTCTTCAC	189
RSV/G protein	GGGGCAAATGCAAACATGT	GGTATTCTTTTGCATATAGC	621
HIF-1α	CAGAAGATACAAGTAGCCTC	CTGCTGGAATACTGTAACTG	673
TGF-β1	CAGCAACAATTCCTGGCGATA	AAGGCGAAAGCCCTCAATTT	135
G3PDH	ACCACAGTCCATGCCATCAC	TCCACCACCCTGTTGCTGTA	452

TABLE 4: Primers of RT–PCR.

Western blot analysis

The hTERT-transfected HNECs were scraped from a 60-mm dish containing 300 μl of buffer (1 mM $NaHCO_3$ and 2 mM phenylmethylsulfonyl fluoride), collected in microcentrifuge tubes, and then sonicated for 10 s. The protein concentrations of the samples were determined using a bicinchoninic acid protein assay reagent kit (Pierce Chemical Co., Rockford, IL). Aliquots of 15 μl of protein per lane for each sample were separated by electrophoresis in 4–20% SDS polyacrylamide gels (Daiichi Pure Chemicals, Tokyo, Japan) and electrophoretically transferred to a nitrocellulose membrane (Immobilon; Millipore, Bedford, UK). The membrane was saturated for 30 min at room temperature with blocking buffer (25 mM Tris, pH 8.0, 125 mM NaCl, 0.1% Tween 20, and 4% skim milk) and incubated with anti–phospho-pan-PKC, anti–pan-PKC, anti–phospho-PKCδ, anti-PKCδ, anti–phospho-NFκB, anti-NFκB, anti–JAM-A, anti-actin, anti-occludin, anti-claudin-1, -4, -7, anti–E-cadherin, anti–HIF-1-α, and anti–RSV/G protein antibodies (Table 2) at room temperature for 1 h. Then it was incubated with horseradish peroxidase–conjugated anti–mouse and anti–rabbit IgG antibodies at room temperature for 1 h. The immunoreactive bands were detected using an enhanced chemiluminescence Western blotting system.

Immunocytochemistry

hTERT-transfected HNECs grown in 35-mm glass-coated wells (Iwaki, Chiba, Japan), were fixed with cold acetone and ethanol (1:1 vol:vol) at –20°C for 10 min. After rinsing in phosphate-buffered saline (PBS), the cells were incubated with anti–RSV/G and /F proteins, and anti-occludin, anti–claudin-4, anti–ZO-1, anti–JAM-A, anti–E-cadherin antibodies (Table 2) overnight at 4°C. Alexa Fluor 488 (green)-conjugated anti–rabbit IgG and Alexa Fluor 592 (red)-conjugated anti–mouse IgG (Invitrogen) were used as secondary antibodies. The specimens were examined and photographed with an Olympus IX 71 inverted microscope (Olympus, Tokyo, Japan) and a confocal laser scanning microscope (LSM510; Carl Zeiss, Jena, Germany).

SEM

Cells grown on coated coverslips were fixed with 2.5% glutaraldehyde/0.1 M PBS (pH 7.3) overnight at 4°C. After several rinses with PBS, the cells were postfixed in 1% osmium tetroxide at 4°C for 3 h and then rinsed with distilled water, dehydrated in a graded ethanol series, and freeze-dried. The specimens were sputter-coated with platinum and observed with a scanning electron microscope (S-4300; Hitachi, Tokyo, Japan) operating at 10 kV.

TEM

The cells were fixed in 2.5% glutaraldehyde/0.1 M PBS (pH 7.3) overnight at 4°C, postfixed in 2% osmium tetroxide in the same buffer, dehydrated in a graded ethanol series, and embedded in Epon 812. Ultrathin sections were then cut on a Sorvall Ultramicrotome MT-5000. The sections were stained with uranyl acetate followed by lead citrate and examined at 60 kV with a JEM transmission electron microscope (JEOL, Tokyo, Japan).

Freeze-fracture analysis

For the freeze-fracture technique, the cells grown on 60-mm dishes were centrifuged into pellets and then immersed in 40% glycerin solution after fixation in 2.5% glutaraldehyde/0.1 M PBS. The specimens were fractured at –150°C to –160°C in a JFD-7000 freeze-fracture device (JEOL) and replicated by deposition of platinum/carbon from an electron beam gun positioned at a 45° angle followed by carbon applied from overhead. Replicas were examined at 100 kV with a JEM transmission electron microscope (JEOL). After the replicas were thawed, they were floated on filtered 10% sodium hypochlorite solution for 30 min in Teflon dishes. They were then washed in distilled water for 30 min, mounted on copper grids, and examined at an acceleration voltage of 100 kV with a JEOL-1200EX transmission electron microscope (JEOL). Morphometric analysis was performed on six freeze-fracture replica images of each one, which were printed at a final magnification of 20,000×. The mean number of tight junction strands was determined by doing numerous counts along a line drawn perpendicular to the junctional axis at 200-nm intervals (Stevenson *et al.*, 1988).

Measurement of TER

hTERT-transfected HNECs were cultured to confluence on inner chambers of 12-mm Transwell inserts with 0.4-μm-pore-size filters (Corning Life Sciences). TER was measured using an EVOM voltameter with an ENDOHM-12 (World Precision Instruments, Sarasota, FL) on a heating plate (Fine, Tokyo, Japan) adjusted to 37°C. The values were expressed in standard units of ohms per square centimeter and presented as the mean ± SD. For calculation, the resistance of blank filters was subtracted from that of filters covered with cells.

GeneChip analysis

Microarray slides were scanned using a 3D-Gene human 25k. (TORAY, Tokyo, Japan), and microarray images were automatically analyzed using AROS, version 4.0 (Operon Biotechnologies, Tokyo, Japan).

MTT assay

The cells plated on 24-well tissue culture plates (BD Labware, Franklin Lakes, NJ) were treated with 0.1–2 μg/ml *C. perfringens* enterotoxin for 1 h. The cell survival was evaluated with the colorimetric assay using an MTT Cell Growth Assay Kit (Millipore, Billerica, MA), according to the manufacturer's recommendations.

Data analysis

Signals were quantified using Scion Image Beta 4.02 Win (Scion, Frederick, MD). Each set of results shown is representative of at least three separate experiments. Results are given as means ± *SEM.*

Differences between groups were tested by analysis of variance followed by a post hoc test and an unpaired two-tailed Student's *t* test and considered to be significant when $p < 0.05$.

ACKNOWLEDGMENTS

We thank Emi Suzuki for her technical support and Yukihiro Somekawa (Sapporo Hospital of Hokkaido Railway Company) and Katsushi Asano (KKR Sapporo Medical Center Tonan Hospital) for their material support. This work was supported by the Suhara Memorial Foundation, the Pancreas Research Foundation of Japan, Grants-in-Aid from the National Project "Knowledge Cluster Initiative" (2nd stage, "Sapporo Biocluster Bio-S"), Program for Developing the Supporting System for Upgrading Education and Research, the Ministry of Education, Culture, Sports, Science, and Technology, and the Ministry of Health, Labor, and Welfare of Japan.

REFERENCES

Bitko V, Velazquez A, Yang L, Yang YC, Barik S (1997). Transcriptional induction of multiple cytokines by human respiratory syncytial virus requires activation of NF-kappa B and is inhibited by sodium salicylate and aspirin. Virology 232, 369–378.

Bitko V, Barik S (1998). Persistent activation of RelA by respiratory syncytial virus involves protein kinase C, underphosphorylated IkBb, and sequestration of protein phosphatase 2A by the viral phosphoprotein. J Virol 72, 5610–5618.

Campbell JA, Schelling P, Wetzel JD, Johnson EM, Forrest JC, Wilson GA, Aurrand-Lions M, Imhof BA, Stehle T, Dermody TS (2005). Junctional adhesion molecule a serves as a receptor for prototype and field-isolate strains of mammalian reovirus. J Virol 79, 7967–7978.

Chen W, Monick MM, Carter AB, Hunninghake GW (2000). Activation of ERK2 by respiratory syncytial virus in A549 cells is linked to the production of interleukin 8. Exp Lung Res 26, 13–26.

Cohen CJ, Shieh JT, Pickles RJ, Okegawa T, Hsieh JT, Bergelson JM (2001). The coxsackievirus and adenovirus receptor is a transmembrane component of the tight junction. Proc Natl Acad Sci USA 98, 15191–15196.

Collins PL, Mottet G (1991). Post-translational processing and oligomerization of the fusion glycoprotein of human respiratory syncytial virus. J Gen Virol 72, 3095–3101.

Evans MJ, von Hahn T, Tscherne DM, Syder AJ, Panis M, Wšlk B, Hatziioannou T, McKeating JA, Bieniasz PD, Rice CM (2007). Claudin-1 is a hepatitis C virus co-receptor required for a late step in entry. Nature 446, 801–805.

Gibbs JD, Ornoff DM, Igo HA, Zeng JY, Imani F (2009). Cell cycle arrest by transforming growth factor beta1 enhances replication of respiratory syncytial virus in lung epithelial cells. J Virol 83, 12424–12431.

Gower TL, Peeples ME, Collins PL, Graham BS (2001). RhoA is activated during respiratory syncytial virus infection. Virology 283, 188–196.

Gralinski LE, Ashley SL, Dixon SD, Spindler KR (2009). Mouse adenovirus type 1-induced breakdown of the blood-brain barrier. J Virol 83, 398–410.

Guttman JA, Finlay BB (2009). Tight junctions as targets of infectious agents. Biochim Biophys Acta 1788, 832–841.

Holt PG, Strickland DH, Wikström ME, Jahnsen FL (2008). Regulation of immunological homeostasis in the respiratory tract. Nat Rev Immunol 8, 142–152.

Ikenouchi J, Furuse M, Furuse K, Sasaki H, Tsukita S, Tsukita S (2005). Tricellulin constitutes a novel barrier at tricellular contacts of epithelial cells. J Cell Biol 171, 939–945.

Jeffree CE, Brown G, Aitken J, Su-Yin DY, Tan BH, Sugrue RJ (2007). Ultrastructural analysis of the interaction between F-actin and respiratory syncytial virus during virus assembly. Virology 369, 309–323.

Kamekura R *et al.* (2010). Thymic stromal lymphopoietin induces tight junction protein claudin-7 via NF-kappaB in dendritic cells. Histochem Cell Biol 133, 339–348.

Kamekura R *et al.* (2009). Thymic stromal lymphopoietin enhances tight-junction barrier function of human nasal epithelial cells. Cell Tissue Res 338, 283–293.

Kilani MM, Mohammed KA, Nasreen N, Tepper RS, Antony VB (2004). RSV causes HIF-1alpha stabilization via NO release in primary bronchial epithelial cells. Inflammation 28, 245–251.

Koizumi J *et al.* (2008). Protein kinase C enhances tight junction barrier function of human nasal epithelial cells in primary culture by transcriptional regulation. Mol Pharmacol 74, 432–442.

Kurose M *et al.* (2007). Induction of claudins in passaged hTERT-transfected human nasal epithelial cells with an extended life span. Cell Tissue Res 330, 63–74.

Lee JW *et al.* (2007). Protein kinase C-delta regulates the stability of hypoxia-inducible factor-1 alpha under hypoxia. Cancer Sci 98, 1476–1481.

Lee MS, Kim TY, Kim YB, Lee SY, Ko SG, Jong HS, Kim TY, Bang YJ, Lee JW (2005). The signaling network of transforming growth factor beta1, protein kinase Cdelta, and integrin underlies the spreading and invasiveness of gastric carcinoma cells. Mol Cell Biol 25, 6921–6936.

Levine S, Klaiber-Franco R, Paradiso PR (1987). Demonstration that glycoprotein G is the attachment protein of respiratory syncytial virus. J Gen Virol 68, 2521–2524.

Medigeshi GR, Hirsch AJ, Brien JD, Uhrlaub JL, Mason PW, Wiley C, Nikolich-Zugich J, Nelson JA (2009). West Nile virus capsid degradation of claudin proteins disrupts epithelial barrier function. J Virol 83, 6125–6134.

Monick M, Staber J, Thomas K, Hunninghake G (2001). Respiratory syncytial virus infection results in activation of multiple protein kinase C isoforms leading to activation of mitogen-activated protein kinase. J Immunol 166, 2681–2687.

Ogasawara N *et al.* (2010). PPARgamma agonists upregulate the barrier function of tight junctions via a PKC pathway in human nasal epithelial cells. Pharmacol Res 61, 489–498.

Ohkuni T, Kojima T, Ogasawara N, Masaki T, Ninomiya T, Kikuchi S, Go M, Takano K, Himi T, Sawada N (2009). Expression and localization of tricellulin in human nasal epithelial cells in vivo and in vitro. Med Mol Morphol 42, 204–211.

Ploss A, Evans MJ, Gaysinskaya VA, Panis M, You H, de Jong YP, Rice CM (2009). Human occludin is a hepatitis C virus entry factor required for infection of mouse cells. Nature 457, 882–886.

Roberts SR, Compans RW, Wertz GW (1995). Respiratory syncytial virus matures at the apical surfaces of polarized epithelial cells. J Virol 69, 2667–2673.

Sajjan U, Wang Q, Zhao Y, Gruenert DC, Hershenson MB (2008). Rhinovirus disrupts the barrier function of polarized airway epithelial cells. Am J Respir Crit Care Med 178, 1271–1281.

Sawada N, Murata M, Kikuchi K, Tobioka H, Kojima T, Chiba H (2003). Tight junctions and human disease. Med Electron Microsc 36, 147–156.

Schneeberger EE, Lynch RD (2004). The tight junction: a multifunctional complex. Am J Physiol Cell Physiol 286, C1213–C1228.

Schneeberger EE, Lynch RD (1992). Structure, function, and regulation of cellular tight junctions. Am J Physiol 262, L647–L661.

Sieczkarski SB, Brown HA, Whittaker GR (2003). Role of protein kinase C ßII in influenza virus entry via late endosomes. J Virol 77, 460–469.

Stevenson BR, Anderson JM, Goodenough DA, Mooseker MS (1988). Tight junction structure and ZO-1 content are identical in two strains of Madin-Darby canine kidney cells, which differ in transepithelial resistance. J Cell Biol 107, 2401–2408.

Takano K, Kojima T, Go M, Murata M, Ichimiya S, Himi T, Sawada N (2005). HLA-DR- and CD11c-positive dendritic cells penetrate beyond well-developed epithelial tight junctions in human nasal mucosa of allergic rhinitis. J Histochem Cytochem 53, 611–619.

Tregoning JS, Pribul PK, Pennycook AM, Hussell T, Wang B, Lukacs N, Schwarze J, Culley FJ, Openshaw PJ (2010). The chemokine MIP1alpha/CCL3 determines pathology in primary RSV infection by regulating the balance of T cell populations in the murine lung. PLoS One 5, e9381.

Tsukita S, Furuse M (1998). Overcoming barriers in the study of tight junction functions: from occludin to claudin. Genes Cells 3, 569–573.

Tsukita S, Furuse M, Itoh M (2001). Multifunctional strands in tight junctions. Nat Rev Mol Cell Biol 2, 285–293.

Tsutsumi H, Nagai K, Suga K, Chiba Y, Chiba S, Tsugawa S, Ogra PL (1989). Antigenic variation of human RSV strains isolated in Japan. J Med Virol 27, 124–130.

Walmsley SR *et al.* (2005). Hypoxia-induced neutrophil survival is mediated by HIF-1alpha-dependent NF-kappaB activity. J Exp Med 201, 105–115.

Wang SZ, Hallsworth PG, Dowling KD, Alpers JH, Bowden JJ, Forsyth KD (2000). Adhesion molecule expression on epithelial cells infected with respiratory syncytial virus. Eur Respir J 15, 358–366.

Wright PF, Ikizler MR, Gonzales RA, Carroll KN, Johnson JE, Werkhaven JA (2005). Growth of respiratory syncytial virus in primary epithelial cells from the human respiratory tract. J Virol 79, 8651–8654.

Yoboua F, Martel A, Duval A, Mukawera E, Grandvaux N (2010). Respiratory syncytial virus-mediated NF-{kappa}B p65 phosphorylation at serine 536 is dependent on RIG-I, TRAF6, and IKK{beta}. J Virol 84, 7267–7277.

Zhang L, Peeples ME, Boucher RC, Collins PL, Pickles RJ (2002). Respiratory syncytial virus infection of human airway epithelial cells is polarized, specific to ciliated cells, and without obvious cytopathology. J Virol 76, 5654–5666.

JOURNAL OF VIROLOGY, Nov. 2011, p. 11871–11882 Vol. 85, No. 22
0022-538X/11/$12.00 doi:10.1128/JVI.05067-11

The SI Strain of Measles Virus Derived from a Patient with Subacute Sclerosing Panencephalitis Possesses Typical Genome Alterations and Unique Amino Acid Changes That Modulate Receptor Specificity and Reduce Membrane Fusion Activity▽‡

Fumio Seki,[1]* Kentaro Yamada,[1]† Yuichiro Nakatsu,[1] Koji Okamura,[2] Yusuke Yanagi,[2] Tetsuo Nakayama,[3] Katsuhiro Komase,[1] and Makoto Takeda[1]

Department of Virology 3, National Institute of Infectious Diseases, Tokyo,[1] Department of Virology, Faculty of Medicine, Kyushu University, Fukuoka,[2] and Laboratory of Viral Infection I, Kitasato Institute for Life Sciences, Kitasato University, Tokyo,[3] Japan

Received 10 May 2011/Accepted 31 August 2011

Subacute sclerosing panencephalitis (SSPE) is a fatal sequela associated with measles and is caused by persistent infection of the brain with measles virus (MV). The SI strain was isolated in 1976 from a patient with SSPE and shows neurovirulence in animals. Genome nucleotide sequence analyses showed that the SI strain genome possesses typical genome alterations for SSPE-derived strains, namely, accumulated amino acid substitutions in the M protein and cytoplasmic tail truncation of the F protein. Through the establishment of an efficient reverse genetics system, a recombinant SI strain expressing a green fluorescent protein (rSI-AcGFP) was generated. The infection of various cell types with rSI-AcGFP was evaluated by fluorescence microscopy. rSI-AcGFP exhibited limited syncytium-forming activity and spread poorly in cells. Analyses using a recombinant MV possessing a chimeric genome between those of the SI strain and a wild-type MV strain indicated that the membrane-associated protein genes (M, F, and H) were responsible for the altered growth phenotype of the SI strain. Functional analyses of viral glycoproteins showed that the F protein of the SI strain exhibited reduced fusion activity because of an E300G substitution and that the H protein of the SI strain used CD46 efficiently but used the original MV receptors on immune and epithelial cells poorly because of L482F, S546G, and F555L substitutions. The data obtained in the present study provide a new platform for analyses of SSPE-derived strains as well as a clear example of an SSPE-derived strain that exhibits altered receptor specificity and limited fusion activity.

Measles is an acute highly contagious disease characterized by high fever and a maculopapular rash. Acute measles is accompanied by temporary and severe immunosuppression, and pneumonia caused by secondary bacterial infections is a major cause of measles-related death in children. Subacute sclerosing panencephalitis (SSPE) is a fatal sequela associated with measles. It occurs at a mean latency period of 7 to 10 years after the acute measles stage of development (3, 52). SSPE is caused by persistent infection of the central nervous system (CNS) with measles virus (MV), and suffering from acute measles at an early age is a risk factor for developing SSPE (17). A recent analysis indicated that the risk of developing SSPE was 22 cases per 100,000 reported cases of acute measles (3).

The causative agent, MV, is an enveloped virus that belongs to the genus *Morbillivirus* in the family *Paramyxoviridae*. MV possesses a nonsegmented, negative-sense RNA genome that includes six linked tandem genes, N, P/V/C, M, F, H, and L. The genome is encapsidated by the nucleocapsid (N) protein and is associated with a viral RNA-dependent RNA polymerase composed of phosphoproteins (P proteins) and large proteins (L proteins) that form a ribonucleoprotein (RNP) complex (12). Two types of glycoprotein spikes, the hemagglutinin (H) and fusion (F) proteins, are expressed on the viral envelope. The H protein is responsible for binding to cellular receptors on the target host cells. The signaling lymphocyte activation molecule (SLAM) expressed on immune system cells functions as the principal receptor for MV (62, 69). We and another group recently demonstrated that certain epithelial cells that form tight junctions express an unidentified receptor for MV that is designated the epithelial cell receptor (ECR) (25, 50, 59). Binding of the H protein to a receptor triggers F protein-mediated membrane fusion of the virus envelope and the host cell plasma membrane (12). These proteins are also expressed on the cell surface and cause cell-to-cell fusion. The matrix (M) protein plays crucial roles in the process of virus assembly via its interaction with both the RNP and the cytoplasmic tails of the glycoproteins. MV strains derived from patients with SSPE (SSPE strains) generally do not express a functional M protein, becoming defective in producing infectious virus particles, and thus spread via cell-to-cell fusion (10, 14–16, 18). In addition, SSPE strains usually have a deletion or an alteration in the cytoplasmic tail of the F protein (4, 9, 31, 44).

* Corresponding author. Mailing address: Department of Virology 3, National Institute of Infectious Diseases, Gakuen 4-7-1, Musashimurayama 208-0011, Tokyo, Japan. Phone: 81-42-561-0771. Fax: 81-42-562-8941. E-mail: fseki@nih.go.jp.

† Present address: Research Promotion Project, Oita University, Oita, Japan.

‡ Supplemental material for this article may be found at http://jvi.asm.org/.

▽ Published ahead of print on 14 September 2011.

The SI strain was isolated in 1976 from a patient with SSPE by cultivating brain tissue biopsy samples with Vero cells (29). The patient was 8 years of age and had suffered from acute measles at 4 years of age (29). The SI strain was found to show neurovirulence, and all animals (mice, hamsters, and guinea pigs) inoculated intracerebrally with the SI strain showed neurological manifestations at 3 to 6 days after inoculation and eventually died (29). Despite these significant characteristics, molecular analyses of the SI strain have been poorly conducted. In the present study, we identified unique characteristics of the SI strain and identified substitutions responsible for the modulated receptor specificity and reduced membrane fusion activity. The present study also obtained data using a genetic engineering system of the SI strain expressing a fluorescent protein. This system could be a new platform for analyses of the molecular bases and pathogenesis of SSPE.

MATERIALS AND METHODS

Cells. BHK/T7-9 cells constitutively expressing T7 RNA polymerase (20) were maintained in Dulbecco's minimum essential medium (DMEM; Sigma, St. Louis, MO) supplemented with 7% fetal bovine serum (FBS). Vero/hSLAM (36) and CV1/hSLAM (58), which constitutively express human SLAM (hSLAM), were maintained in DMEM supplemented with 7% FBS and 0.5 mg/ml Geneticin (G418; Invitrogen Life Technologies, Carlsbad, CA). CHO cells and A549 cells constitutively expressing human SLAM, CHO/hSLAM (62), and A549/hSLAM (57), respectively, were maintained in RPMI medium (Invitrogen) supplemented with 7% FBS and 0.5 mg/ml G418. Vero cells and IMR-32 cells were maintained in DMEM supplemented with 7% FBS and 10% FBS, respectively. H358 (59) and II-18 (49) cells were maintained in RPMI supplemented with 10% FBS. SH-SY5Y cells were maintained in DMEM/F12 (Invitrogen) supplemented with 10% FBS (49, 59).

Plasmid constructions. The first-strand cDNA of the SI strain antigenome was synthesized by reverse transcription of total RNA isolated from Vero/hSLAM cells infected with the SI strain. Eight DNA fragments covering the entire region of the SI strain genome were then generated by PCR. These fragments were cloned into pBluescriptII KS(+) vector (Agilent Technologies, Inc., Santa Clara, CA) in a stepwise manner, generating a plasmid carrying the full-length antigenomic cDNA of the SI strain (detailed procedure provided upon request). A hammerhead ribozyme sequence (HHRz) was added between the T7 promoter sequence and the MV genome cDNA by a combination of PCR procedures using the synthesized DNA (5′-**GTGAATTGTAATACGACTCACTATAGGG***TGTTTG GTCTGATGAGGCCGAAAGGCCGAAACTCCGTAAGGAGTC*ACCAAACA AA-3′; the T7 promoter and HHRz sequences are shown in boldface and italics, respectively, and the MV genome cDNA sequence is underlined). To generate an additional transcriptional unit for a green fluorescent protein (GFP) derived from *Aequorea coerulescens* (AcGFP; Clontech, Palo Alto, CA), a fragment containing the open reading frame (ORF) of AcGFP was amplified by PCR using primer pair 5′-*GGCGCGCC***ATG**GTGAGCAAG-3′ and 5′-*GACGTC***TT** ACTTGTACAGCTCGT-3′ (sequences corresponding to the AscI and AatII sites are shown in italics; sequences corresponding to the initiation and termination codons are shown in boldface). The fragment was combined with the synthesized cDNA fragments containing the region between the H and L protein open reading frames of the IC-B strain by a combination of PCR procedures. The nucleotide sequences of the synthesized cDNA fragments were 5′-**ACTAGT**GAAATAGACA TCAGAATTAAGAAAAACGTAGGGTCCAAGTGGTTTCCCGTT*GGCGCG CC*-3′ and 5′-*GACGTC*TGCCAGTGAACCGATCACATGATGTCACCCAGAC ATCAGGCATACCC**ACTAGT**-3′ (sequences corresponding to SpeI sites are shown in boldface, sequences corresponding to AscI and AatII sites are shown in italics, and sequences corresponding to the gene end [GE] of the H gene and gene start [GS] of the L gene are underlined). The fragment containing the transcriptional unit for AcGFP was then inserted into the SpeI site between the H and L genes. The generated construct was named pHHRz-SI-AcGFP. Using a similar procedure, the additional transcriptional unit for AcGFP was also inserted into the p(+)MV323 plasmid, which carries the full-length antigenomic cDNA of the IC-B strain (60). The resulting plasmid was named p(+)MV323-AcGFP. A SalI-AatII fragment containing a region of the M, F, and H genes of p(+)MV323-AcGFP was replaced with a corresponding fragment of pHHRz-SI-AcGFP, and the generated construct was named p(+)MV323/SI-MFH-AcGFP. A SalI-BstEII fragment containing a region of the M gene of the pHHRz-SI-AcGFP was replaced with a corresponding fragment of p(+)MV323, and the generated construct was named pHHRz-SI/ICM-AcGFP. To generate support plasmids for the rescue of recombinant MVs from cloned cDNAs, DNA fragments encoding the N, P, and L proteins of the wild-type (wt) MV strains (IC-B or 9301B) were cloned into the pCITE vector (Novagen, Madison, WI), generating pCITE-IC-N, pCITE-IC-PΔC, and pCITEko-9301B-L, respectively. DNA fragments encoding the M proteins of the IC-B and SI strains fused with a red fluorescent protein, mCherry (Clontech), at the carboxyl-terminal end were generated by a combination of PCR procedures and inserted into a mammalian expression vector, pCA7 (32, 57). The resulting plasmids were named pCA7-FR-IC-M-mCherry and pCA7-FR-SI-mCherry, respectively. DNA fragments encoding the F proteins of the IC-B and SI strains were also amplified by PCR and cloned into pCAGGS (32), generating pCAGGS-IC-F and pCAGGS-SI-F, respectively. Similarly, DNA fragments encoding the H proteins of the IC-B and SI strains were amplified and cloned into pCAGGS, generating pCAGGS-IC-H and pCAGGS-SI-H, respectively. By replacing the SalI-XhoI, EcoRI-SalI, KpnI-XhoI, and SalI-KpnI regions of pCAGGS-IC-F with the corresponding region of pCAGGS-SI-F, four plasmids encoding chimeric F proteins between the IC-B and SI strains, designated pCAGGS-IC/SI-F-1, -F-2, -F-3, and -F-4, respectively, were generated. An amino acid substitution, G300E, was introduced into pCAGGS-SI-F, and five other amino acid substitutions, N390M, L482F, S546G, F555L, and I564L, were introduced independently into pCAGGS-IC-H by site-directed mutagenesis using complementary primer pairs.

Antibodies. A mouse monoclonal antibody (MAb) against CD46 (M75) was kindly provided by T. Seya (46). Mouse MAbs against the proteins encoded by MV H (B5), F (C527), and M (A23, A24, A27, A154, A157, A177, B46, A39, A41, A42, A51, and A133) were kindly provided by T. A. Sato (42).

Viruses. BHK/T7-9 cells were transfected with full-length genome plasmids carrying the antigenomes of MV and three support plasmids, pCITE-IC-N, pCITE-IC-PΔC, and pCITEko-9301B-L, by the use of Lipofectamine LTX Plus reagent (Invitrogen). After 2 days, the transfected cells were cocultured with Vero/hSLAM cells. IC323-AcGFP, SI-AcGFP, IC/SI-MFH-AcGFP, and SI/ICM-AcGFP were generated from p(+)MV323-AcGFP, pHHRz-SI-AcGFP, p(+)MV323/SI-MFH-AcGFP, and pHHRz-SI/ICM-AcGFP, respectively. The generated MVs were propagated in Vero/hSLAM cells. Infectious virus-like particles of SI-AcGFP and IC/SI-MFH-AcGFP were prepared by incubating the cells with 5 μg/ml cytochalasin D (Sigma) at 35°C for 30 min, as described previously (19). The infectious virus-like particles were concentrated using PEG-it precipitation solution (System Biosciences Inc., Mountain View, CA). The cell infectious units (CIUs) of the recombinant MVs expressing a fluorescent protein were determined using Vero/hSLAM cells, as described previously (51). To analyze the cytopathic effects (CPEs), monolayers of cells in 6-well cluster plates were infected with 500 CIUs of MV and the cells were observed daily using an Axio Observer.D1 microscope (Carl Zeiss, Jena, Germany).

Virus growth. Monolayers of Vero/hSLAM cells in 24-well plates were infected with recombinant MVs at a multiplicity of infection (MOI) of 0.01 per cell. At various time intervals, cell-free virus was obtained from the culture supernatants, and cell-associated virus was recovered from infected cells in 0.5 ml of DMEM-supplemented 7% FBS by freezing and thawing.

Virus titration. Monolayers of Vero/hSLAM cells in 6-well cluster plates were infected with serially diluted virus samples, incubated for 1 h at 37°C, and overlaid with DMEM containing 7% FBS and 1% agarose. PFU numbers were determined by counting the number of plaques.

Phylogenic tree analysis and Ka/K_s calculation. Nucleotide and amino acid sequence alignments and a phylogenic distance analysis were performed with the ClustalW program (63) at the genomeNet website maintained by the Kyoto University Bioinformatics Center. A phylogenic tree constructed using SI, IC-B, 9301B, WA.USA/17.98, and reference strains (66) was drawn using FigTree software. Ka/K_s calculations were performed using KaKs Calculator version 2.0 software (64). Briefly, using the two nucleotide sequences of each protein-coding region, the nonsynonymous and synonymous substitution rates (Ka and K_s, respectively) were calculated by counting the numbers of nonsynonymous and synonymous sites (NA and NS, respectively) and the numbers of nonsynonymous and synonymous substitutions (MA and MS, respectively). MA/NA and MS/NS represent the Ka and K_s substitution rates, respectively.

Immunofluorescence staining. Monolayers of Vero/hSLAM cells were seeded in 24-well plates or on coverslips in six-well cluster plates. Some monolayers were transfected with expression plasmids encoding M protein tagged with mCherry or not tagged. Other monolayers were infected with recombinant MVs and incubated with 50 μg/ml of a fusion-blocking peptide, Z-D-Phe-Phe-Gly (Peptide Institute Inc., Osaka, Japan), as described previously (41). At 24 h posttransfection or at 2 or 5 days postinoculation (p.i.) (using IC323-AcGFP or SI-AcGFP,

respectively), the cells were fixed and permeabilized with phosphate-buffered saline containing 2.5% formaldehyde and 0.5% Triton X-100. The cells were then stained with a mouse MAb against the M protein for 1 h at room temperature, followed by incubation with an Alexa Fluor 488- or 594-conjugated secondary antibody (Molecular Probes, Eugene, OR) for 1 h at room temperature. The nuclei of the infected cells were stained with 4′,6′-diamidino-2-phenylindole (DAPI; Nacalai Tesque, Kyoto, Japan) at 0.2 μg/ml. The cells were observed using a FluoView FV1000 confocal microscope (Olympus, Tokyo, Japan).

Cell-to-cell fusion assay. CHO/hSLAM, CV1/hSLAM, Vero, H358, or II-18 cells were seeded in 24-well plates, transfected with the H protein-expressing plasmid (0.5 μg) together with the F protein-expressing plasmid (0.5 μg), and incubated in the presence or absence of an anti-CD46 antibody (M75). At 1, 2, or 3 days posttransfection, the cells were fixed with methanol and stained with Giemsa solution (Sigma). The stained cells were observed under an Axio Observer.D1 microscope. To quantify cell-to-cell fusion, monolayers of cells were transfected with H protein-expressing plasmid (0.3 μg) and F protein-expressing plasmid (0.3 μg) together with a red fluorescent protein (mCherry)-expressing plasmid (0.3 μg). At 48 h posttransfection, areas expressing mCherry autofluorescence were measured using an Axio Observer.D1 microscope and ImageJ software (http://rsbweb.nih.gov/ij/index.html). Statistical analyses were performed using Microsoft Excel version 14.1.2 software.

Flow cytometry. CHO/hSLAM cells were transfected with the H or F protein-expressing plasmid (0.5 μg). At 24 h posttransfection, the cells were incubated with mouse MAbs B5 and C527 specific for the H and F proteins, respectively, followed by incubation with an Alexa Fluor 488-conjugated goat anti-mouse secondary antibody (Molecular Probes). The cells were analyzed using a FACSCalibur flow cytometer (Becton Dickinson, Franklin Lakes, NJ).

Minigenome assay. BHK/T7-9 cells were transfected with 0.2 μg of p18MGFLuc01 minigenome plasmid (23) together with 0.2 μg of pCITE-IC-N and various amounts of pCITE-IC-PΔC and pCITEko-9301B-L. At 48 h posttransfection, the enzymatic activity of firefly luciferase was measured using a Dual Glo luciferase assay system (Promega, Madison, WI) and a Mithras LB 940 luminometer (Berthold Technologies, Bad Wildbad, Germany).

Nucleotide sequence accession number. The nucleotide sequence of the SI strain is available under GenBank accession number JF791787.

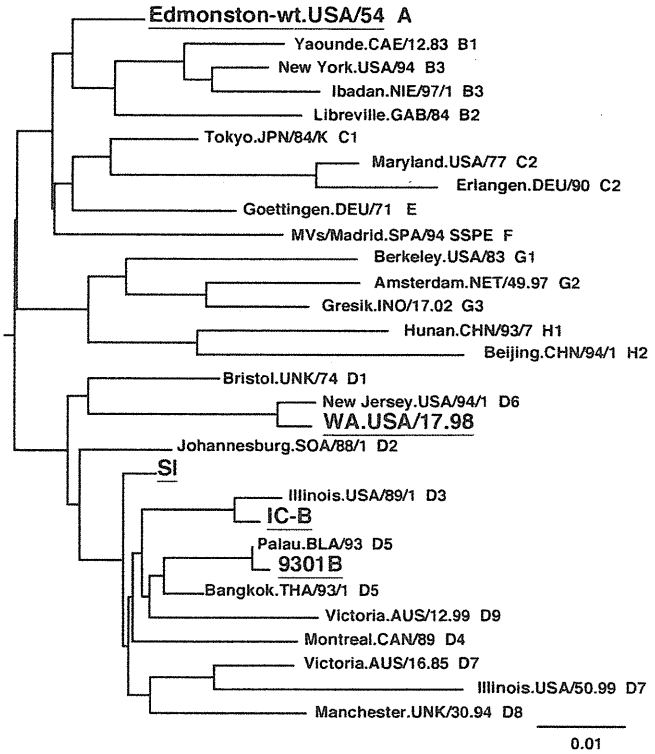

FIG. 1. Phylogenic tree drawn on the basis of the 450-nucleotide sequence that encodes the carboxyl-terminal 150 amino acids of the N protein. The names of the strains used for sequence comparisons in this study (Edmonston-wt, SI, IC-B, 9301B, and WA.USA/17.98) are underlined.

RESULTS

Characterization of the genome of the SI strain. We determined the entire genome nucleotide sequence of the SI strain. A phylogenic tree drawn on the basis of the 450-nucleotide sequence that encodes the carboxyl-terminal 150 amino acids of the N protein showed that the SI strain was classified into clade D but did not belong to a specific genotype (Fig. 1). Genotype analyses performed using a program at a website for measles nucleotide surveillance (MeaNS) (http://www.hpa-bioinformatics.org.uk/Measles/Public/Web_Front/main.php) confirmed the data for the phylogenic tree analysis (see Table S1 in the supplemental material). The entire genome nucleotide sequence of the SI strain was compared with those of three other strains in clade D, strain IC-B (genotype D3; GenBank accession number NC_001498), strain 9301B (genotype D5; GenBank accession number AB012948), and strain WA.USA/17.98 (genotype D6; GenBank accession number DQ227321) (2, 54, 61). The nucleotide sequences of the regulatory regions (i.e., the gene start, gene end, and integenic sequences) (38) were highly conserved in the SI strain genome. As indicated in previous reports (9, 11, 68), highly biased uracil-to-cystine substitutions were observed in the M gene (see Table S2 in the supplemental material). As also observed for other SSPE strains, nonsynonymous substitutions were accumulated in the M protein reading frame of the SI strain (see Fig. S1 in the supplemental material). The data for the comparison between the SI and IC-B strains are shown in the present paper, but similar results were obtained in the comparisons between the SI and other clade D MV strains. The Ka/K_s ratios were analyzed to reveal differences between the SI and clade D MV strains (IC/SI, 9301/SI, and WA98/SI) and between the Edmonston wild-type (wt) strain (genotype A; GenBank accession number AF266288) and clade D MV strains (IC/Edwt, 9301/Edwt, and WA98/Edwt) (37) (the phylogenic tree in Fig. 1 shows the relationships among the SI, IC-B, 9301B, WA.USA/17.98, and Edmonston wt strains). The data of comparisons between the Edmonston wt and clade D MV strains mostly reflect the selection pressure that operated during the natural evolution of wt MVs, while the data showing comparisons between the SI and clade D MV strains reflect the selection pressure that operated during persistent infection in the brain in addition to the natural evolution of MV. Previously, a similar study was performed by Woelk et al. (67). For the M protein reading frame, the Ka/K_s ratios in the comparisons between the Edmonston wt and clade D MV strains were ~0.03, whereas the ratios in the comparisons between the SI and clade D MV strains were 11 to 12 times greater than those observed in comparisons between the Edmonston wt and clade D MV strains (Table 1), confirming that a dynamic selection or a reduced stabilizing selection pressure operated for the M protein of the SI strain, as observed for other SSPE strains (67). Similarly, although the amino acid sequence of the F protein was highly conserved during the natural evolution of MV (Ka/K_s = 0.0000 ~ 0.0359), this was not the case during persistent infection in the brain (Ka/K_s = 0.1825 ~ 0.2504) (Table 1). Compared with those of IC-B, 12 amino acid changes were found in the F protein of the SI strain, including

TABLE 1. K_s, Ka, and Ka/K_s values from comparisons of Edmonston wild-type, IC-B, 9301B, WA.USA/17.98, and SI strains[a]

Protein reading frame	Gene region(s)	Nucleotides[b]	K_s		Ka		Ka/K_s	
			IC(D3)/Edwt, 9301(D5)/Edwt, WA98(D6)/Edwt	IC(D3)/SI, 9301(D5)/SI, WA98(D6)/SI	IC(D3)/Edwt, 9301(D5)/Edwt, WA98(D6)/Edwt	IC(D3)/SI, 9301(D5)/SI, WA98(D6)/SI	IC(D3)/Edwt, 9301(D5)/Edwt, WA98(D6)/Edwt	IC(D3)/SI, 9301(D5)/SI, WA98(D6)/SI
N		1–1578	0.0790, 0.0960, 0.1033	0.0512, 0.0703, 0.1218	0.0117, 0.0113, 0.0092	0.0046, 0.0050, 0.0075	0.1486, 0.1178, 0.0892	0.0898, 0.0712, 0.0618
P	P	1–1524	0.0416, 0.0443, 0.0330	0.0246, 0.0273, 0.0330	0.0114, 0.0176, 0.0132	0.0079, 0.0141, 0.0096	0.2740, 0.3981, 0.3982	0.3195, 0.5150, 0.2918
	P/C	22–582	0.0222, 0.0223, 0.0297	0.0073, 0.0074, 0.0147	0.0191, 0.0239, 0.0215	0.0024, 0.0071, 0.0047	0.8596, 1.0739, 0.7241	0.3217, 0.9645, 0.3212
	P/V	691–903	0.0178, 0.0177, 0	0.0177, 0.0176, 0	0, 0.0064, 0.0129	0.0195, 0.0262, 0.0327	0, 0.3643, NA[c]	1.0991, 1.4842, NA
	P′	1–21 + 583–690 + 904–1524	0.0648, 0.0704, 0.0465	0.0405, 0.0461, 0.0585	0.0088, 0.0160, 0.0071	0.0088, 0.0160, 0.0071	0.1361, 0.2272, 0.1516	0.2179, 0.3472, 0.1206
C		1–561	0.0464, 0.0705, 0.0543	0.0075, 0.0305, 0.0151	0.0119, 0.0095, 0.0143	0.0024, 0, 0.0047	0.2561, 0.1345, 0.2629	0.3132, 0, 0.3127
V	V trans[d]	690–902	0, 0.0217, 0.0439	0.0434, 0.0667, 0.0902	0.0063, 0, 0	0.0063, 0, 0	NA, 0, 0	0.1449, 0, 0
M		1–1008	0.0842, 0.0936, 0.0892	0.2135, 0.2134, 0.2141	0.0026, 0.0026, 0.0026	0.0758, 0.0758, 0.0772	0.0310, 0.0279, 0.0293	0.3551, 0.3552, 0.3606
F		1–1653	0.0566, 0.0627, 0.0675	0.0355, 0.0459, 0.0621	0, 0.0024, 0.0024	0.0089, 0.0113, 0.0113	0, 0.0359, 0.0357	0.2504, 0.2470, 0.1825
H		1–1854	0.0902, 0.0877, 0.0724	0.0675, 0.0651, 0.0907	0.0114, 0.0100, 0.0092	0.0085, 0.0071, 0.0135	0.1263, 0.1135, 0.1276	0.1262, 0.1089, 0.1490
L		1–6549	0.0801, 0.0927, 0.0822	0.0601, 0.0687, 0.0781	0.0047, 0.0051, 0.0049	0.0050, 0.0054, 0.0058	0.0584, 0.0548, 0.0594	0.0828, 0.0782, 0.0739

[a] Edwt, Edmonston wild type; IC(D3), IC-B; 9301(D5), 9301B; WA98(D6), WA.USA/17.98.
[b] The first nucleotide of the initiation codon for each open reading frame is taken as 1.
[c] NA, not applicable.
[d] V trans is the C-terminal region unique to the V protein.

a nonsense mutation at amino acid position 532 (Table 2). These changes in the F protein are typical of SSPE strains (4, 9, 31, 44). For the N, H, and L protein reading frames, in contrast, the Ka/K_s ratios revealed by the comparisons between the SI and clade D MV strains were similar to those observed between the Edmonston wt and clade D MV strains (Table 1). These data indicated that similar levels of stabilizing selection pressure operated for the N, H, and L protein reading frames of the SI strain during the persistent infection in the brain. For the P gene, it was not simple to assess the data for the Ka and K_s values, since the gene contains overlapping reading frames. Nonetheless, it was evident that both the C and V nonstructural proteins were highly conserved during the persistent infection in the brain. For the C protein-reading frame, the Ka values for the IC/SI and WA93/SI comparisons were as much as 3 to 5 times lower than those for the IC/Edwt and WA93/SI comparisons (Table 1). Indeed, no amino acid substitution was found in the C protein of the SI strain compared with that of the 9301B strain. Similarly, no amino acid substitution was found in the V protein-unique region of the SI strain compared with that of the WA.USA/17.98. strain. The V protein-unique region of the 9301B strain also had the same amino acid sequence as those of the SI and WA.USA/17/98 strains except that the 9301B V protein possessed an additional single amino acid at the carboxyl-terminal end, because it terminated one codon later (since this additional codon was not included in calculation, the Ka of 9301/SI comparison was zero [Table 1]). These data suggested that both the C and V proteins played important roles in the survival of the SI strain in the brain.

Generation of a recombinant SI strain expressing a fluorescent protein by establishment of an efficient MV rescue system. The SI strain did not produce cell-free infectious particles and spread poorly in cell cultures (data not shown). In addition, a CPE was barely detectable in some cultured cells, although the SI strain replicated in them (data not shown). Many studies have shown that the use of recombinant viruses genetically engineered to express a fluorescent protein is greatly advantageous for monitoring virus infections, especially when the virus infection shows a small or weak CPE. Therefore, we decided to generate a recombinant SI strain expressing a fluorescent protein. A full-length genome cDNA of the SI strain possessing an additional transcriptional unit encoding AcGFP between the H and L genes was generated and inserted into the pBluescript vector downstream of the T7 promoter (Fig. 2). The T7 promoter was followed by three guanines that enhance the transcription efficiency (Fig. 2). Since these guanines produce extra guanine residues at the 5′ end of the synthesized MV antig-

TABLE 2. Amino acid substitutions in the F proteins among the IC, SI, and Edmonston strains

Amino acid no.	Amino acid substitution(s) or category		
	IC	SI	Ed
78	R	G	R
165	R	K	R
167	A	T	A
187	I	V	I
242	I	T	I
246	L	F	L
247	E	K	E
268	G	D	G
300	E	G	E
487	M	I	M
532	R	Stop	R
533–550	18 aa[a]	Deletion	18 aa

[a] aa, amino acids.

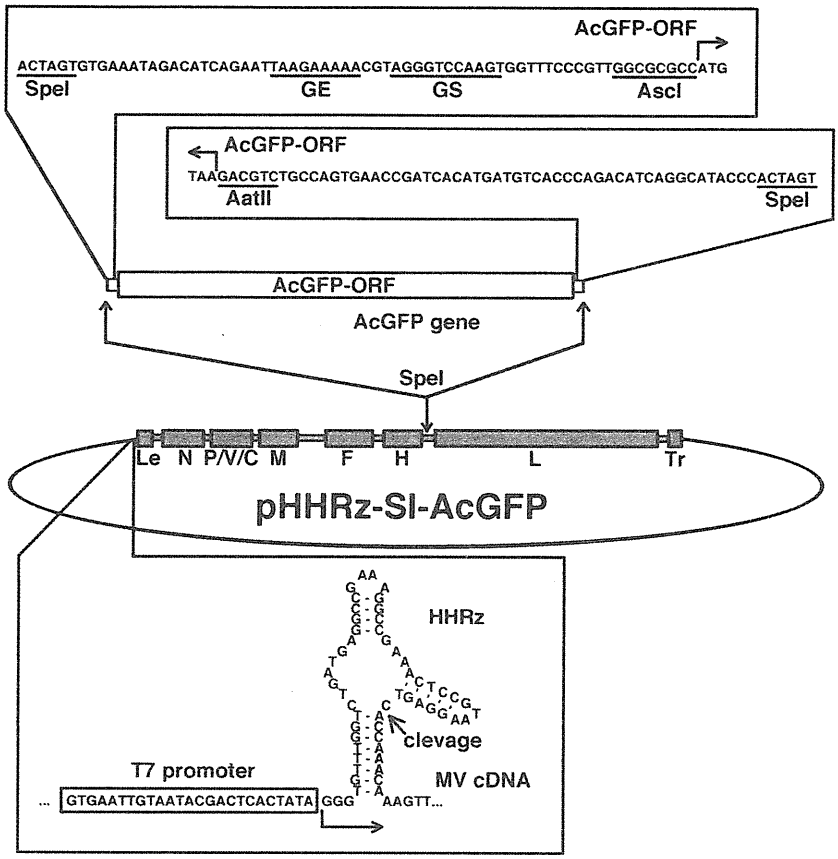

FIG. 2. Diagram of the genome plasmid with insertion of an additional transcriptional unit and the HHRz sequence. Transcriptional regulatory regions (gene end [GE], intergenic, and gene start [GS] sequences) and the coding sequence for AcGFP (AcGFP-ORF) were inserted at the junction between the H and L genes by the use of appropriate restriction enzyme recognition sites (SpeI, AscI, and AatII). The recombinant genome also possesses an HHRz upstream the authentic virus genome.

enome, a precise 5′ end for the MV antigenome was created by inserting HHRz between the three guanines and the first viral nucleotide (Fig. 2). The resulting full-length genome plasmid was designated pHHRz-SI-AcGFP. BHK/T7-9 cells, which represent a baby hamster kidney (BHK) cell-derived clone constitutively expressing T7 RNA polymerase (20) (kindly provided by M. Sugiyama and N. Ito), has been shown to be highly potent for initiating the replication cycles of other negative-strand RNA viruses from cloned cDNAs (20, 48). By the use of previously reported methods of studies employing BHK/T7-9 cells (48), the cDNAs of the N, P, and L genes of MV were inserted into the pCITE vector; the resulting plasmids were termed pCITE-IC-N, pCITE-IC-PΔC, and pCITEko-9301B-L, respectively. These plasmids were designed to create an internal ribosome entry site at the 5′ terminus of the N, P, and L mRNAs. Since the ratios of the plasmids expressing the N, P, and L proteins were previously reported to be critical for the initiation of infectious cycles of paramyxoviruses from cloned cDNAs (13, 21, 26), the optimal ratio for these plasmids was determined using a minireplicon assay for MV (23). The analyses indicated that 0.20, 0.15, and 0.40 μg of pCITE-IC-N, pCITE-IC-PΔC, and pCITEko-9301B-L, respectively, were optimal for the expression of the MV minireplicon gene (luciferase) in BHK/T7-9 cells cultured in a 24-well cluster plate (see Table S3 in the supplemental material). When BHK/T7-9 cells cultured in a 6-well cluster plate were transfected with 5.0 μg of pHHRz-SI-AcGFP together with three support plasmids (0.80, 0.60, and 1.60 μg of pCITE-IC-N, pCITE-IC-PΔC, and pCITEko-9301B-L, respectively), infectious cycles of rSI-AcGFP were efficiently initiated from pHHRz-SI-AcGFP. Subsequently, the recombinant SI strain expressing AcGFP

TABLE 3. Detection of the M protein by an indirect immunofluorescence assay

MAb clone no.	Antigenic site	Assay result			
		IC323-AcGFP	SI-AcGFP	IC-M-mCherry	SI-M-mCherry
A23	II	+	−	+	−
A24	II	+	−	+	−
A27	II	+	−	+	−
A154	II	+	−	+	−
A157	II	+	−	+	−
A177	II	+	−	+	−
B46	II	+	−	+	−
A39	III	+	−	+	−
A41	III	+	−	+	−
A42	III	+	−	+	−
A51	III	+	−	+	−
A133	IV	+	−	+	−

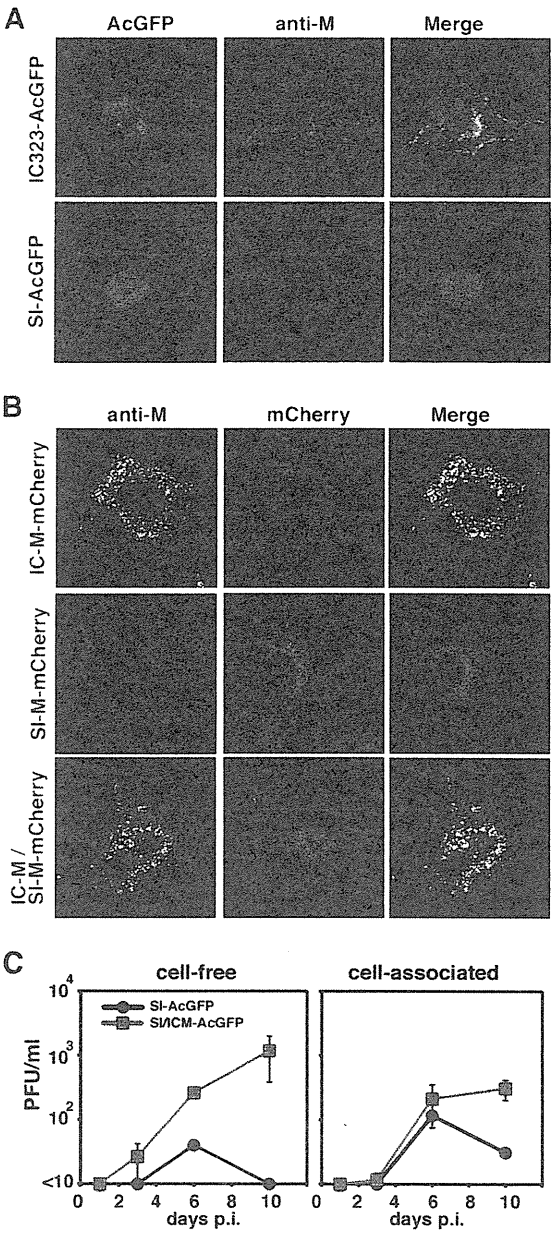

FIG. 3. Distribution of the M protein and effect on viral growth of strain SI possessing the IC-M gene. (A) Distribution of the M protein in cells infected with recombinant MV. Vero/hSLAM cells were infected with IC323-AcGFP or SI-AcGFP. At 2 (IC323-AcGFP) or 5 (SI-AcGFP) days postinfection, the cells were stained with an anti-M protein MAb (A42) and an Alexa Fluor 594-conjugated anti-mouse secondary antibody. The nuclei were stained with DAPI (blue). (B) Distribution of the mCherry-fused M protein. Vero/hSLAM cells were transfected with the M protein-expressing plasmids IC-M-mCherry, SI-M-mCherry, and IC-M plus SI-M-mCherry. At 1 day posttransfection, the cells were stained with an anti-M protein MAb (A42) and an Alexa 488-conjugated anti-mouse secondary antibody. The cells were observed under a confocal microscope. (C) Replication kinetics of recombinant MVs. Vero/hSLAM cells were infected with recombinant MVs at an MOI of 0.01, and infectious titers in culture medium (cell-free) and cells (cell-associated) were determined at 1, 3, 6, and 10 days p.i. Data represent the means ± standard deviations (SD) of results from triplicate samples.

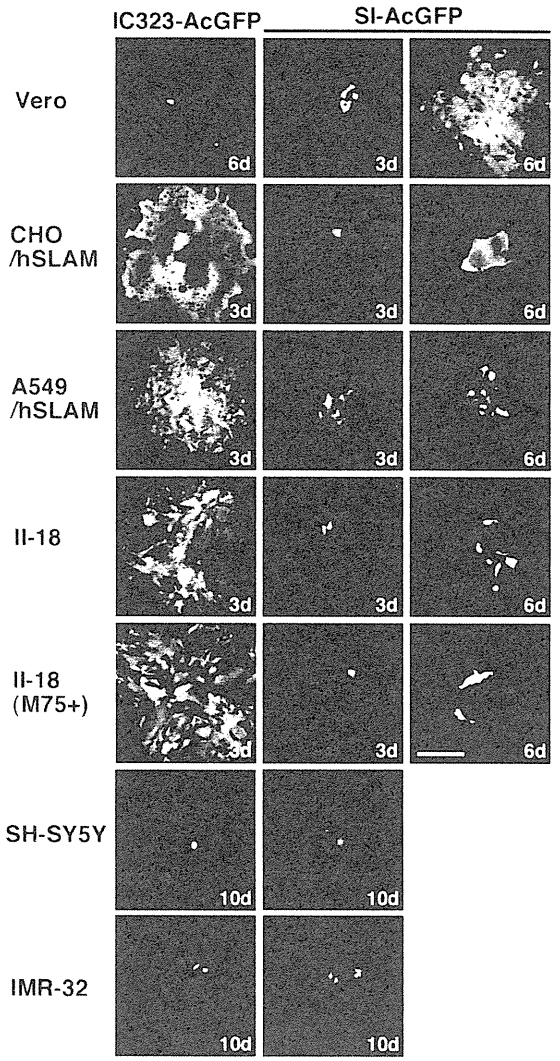

FIG. 4. AcGFP autofluorescence in cells infected with IC323-AcGFP and SI-AcGFP. Vero, CHO/hSLAM, A549/hSLAM, II-18, SH-SY5Y, and IMR-32 cells were infected with IC323-AcGFP or SI-AcGFP. Some II-18 cells were incubated with an anti-CD46 MAb (M75). The cells were observed under a fluorescence microscope at the indicated days (d). Bar, 0.20 mm.

(rSI-AcGFP) was maintained in Vero/hSLAM cells cocultured with BHK/T7-9 cells.

Properties of the M protein of the SI strain. Using various MAbs against the M protein (42), an indirect immunofluorescence assay was performed. A total of 12 MAbs that have been shown to recognize antigenic sites II, III, and IV of the M protein were used (42) (Table 3). A recombinant IC323 strain expressing AcGFP (IC323-AcGFP) was generated and used as a control. The IC323 strain is a recombinant MV based on the wt IC-B strain (60). In cells infected with IC323-AcGFP, all the MAbs detected the M protein (Fig. 3A and Table 3). However, in cells infected with the SI or rSI-AcGFP strains, all the MAbs failed to detect the M protein (Fig. 3A and Table 3 and data not shown). These data suggested a lack of M protein expression in cells infected with the SI and rSI-AcGFP strains. Sato et al. (43) also previously showed that M protein expression

TABLE 4. Amino acid substitutions in the H proteins of the IC, SI, and Edmonston strains

Amino acid no.	Amino acid substitution		
	IC	SI[a]	Ed[b]
7	R	Q*	R
71	H	R*	H
174	A	A	T
176	A	A	T
211	S	S	G
235	G	E	E
243	G	G	R
252	H	H	Y
276	F	F	L
284	F	F	L
296	F	F	L
302	R	R	G
334	R	Q	Q
390	N	M*	I
416	N	N	D
446	T	S	S
481	N	N	Y
482	L	F*	L
484	T	T	N
546	S	G*	S
555	F	L*	F
564	I	L*	I
575	K	Q	Q
600	V	V	E

[a] Asterisks indicate amino acids unique to the SI strain.
[b] Edmonston strain; GenBank accession number K01711.

The SI strain exhibits limited syncytium-forming activity. Various types of cells were infected with SI-AcGFP and IC323-AcGFP. IC323-AcGFP poorly entered Vero cells ($SLAM^-$/$CD46^+$) and did not produce a syncytium (Fig. 4). On the other hand, SI-AcGFP was able to produce syncytia in Vero cells (Fig. 4). Table 4 shows the amino acid substitutions in the H protein. Among them, the S546G substitution is the one that probably contributed to the ability of SI-AcGFP to produce syncytia in Vero cells, because this mutation allows MV to use CD46 as a receptor (69). On the other hand, SI-AcGFP failed to produce syncytia in II-18 cells (ECR^+, $CD46^+$), although IC323-AcGFP replicated and produced syncytia in these cells efficiently (Fig. 4). An MAb against CD46 (M75) had a neutral effect on the SI-AcGFP infection of II-18 cells. Similar results were obtained for the infection of SLAM-positive cells (CHO/hSLAM, A549/hSLAM). SI-AcGFP produced syncytia poorly in these cells, whereas IC323-AcGFP produced syncytia very efficiently. These data demonstrate that the SI strain has limited activity in inducing syncytia in SLAM- or ECR-expressing cells, although it has acquired the ability to use CD46 as an alternative receptor. Although three neural cell lines (SK-N-SH, IMR-32, and SH-SY5Y) were infected with SI-AcGFP and IC323-AcGFP, no syncytia were observed in these cells (Fig. 4 and data not shown).

The membrane-associated protein genes (M, F, and H) determine the growth phenotype of the SI strain. The amino acid sequences of the RNP component proteins (N, P, and L proteins) of the SI and IC-B strains were expressed in cells by the use of expression plasmids. The carboxyl termini of the M proteins were tagged with mCherry red fluorescent protein. All the MAbs detected the IC-B strain-derived M protein despite the mCherry tag (Table 3). In contrast, none of the MAbs detected the SI strain-derived M protein, although bright mCherry fluorescence was detected in these cells (Fig. 3B and Table 3). These data indicated that the antigenicity of the M protein of the SI strain was totally different from that of the M protein of the IC-B strain and that none of the MAbs recognizing antigenic sites II, III, and IV reacted with the M protein of the SI strain. Therefore, we could not reach a conclusion as to whether the M protein was expressed in cells infected with the SI strain. However, analyses using the expression plasmids demonstrated that, unlike the M protein of the IC-B strain, the M protein of the SI strain was distributed homogeneously in cells (Fig. 3B). The M protein of the IC-B strain was distributed beneath the plasma membrane and formed small dots in the cytoplasm (Fig. 3B). To elucidate the functional difference between the IC-B and SI strains with respect to the M gene, we generated a recombinant MV with a modified SI strain genome in which the M gene was replaced with the M gene of the IC-B strain. The resulting recombinant MV was designated SI/ICM-AcGFP. A growth kinetics analysis showed that, unlike SI-AcGFP, SI/ICM-AcGFP produced cell-free virus well and the cell-free virus titer of SI/ICM-AcGFP was ~1,000 times higher than that of the SI-AcGFP at 10 days p.i. (Fig. 3C). The result demonstrated that SI-M protein was less involved in the budding stage. With these data, we concluded that the SI strain does not express a functional M protein.

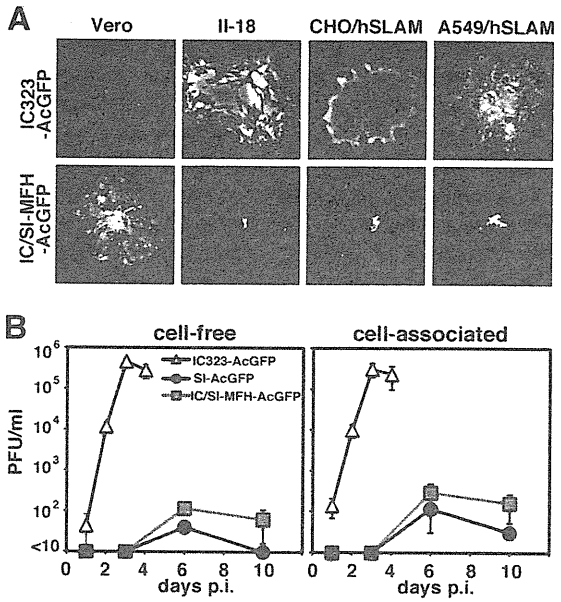

FIG. 5. Effect on viral growth of strain IC possessing the SI-MFH gene in various cell lines. (A) AcGFP fluorescence in cells infected with recombinant MVs. Vero, II-18, CHO/hSLAM, and A549/hSLAM cells were infected with IC323-AcGFP or IC323/SI-MFH-AcGFP. The cells were observed under a fluorescence microscope at 3 (II-18, CHO/hSLAM, and A549/hSLAM) and 6 (Vero) days postinfection. (B) Replication kinetics of recombinant MVs. Vero/hSLAM cells were infected with recombinant MVs at an MOI of 0.01. At various time intervals, infectious titers in culture medium (cell-free) and cells (cell-associated) were determined. Data represent the means ± standard deviations (SD) of the results of experiments performed with triplicate samples.

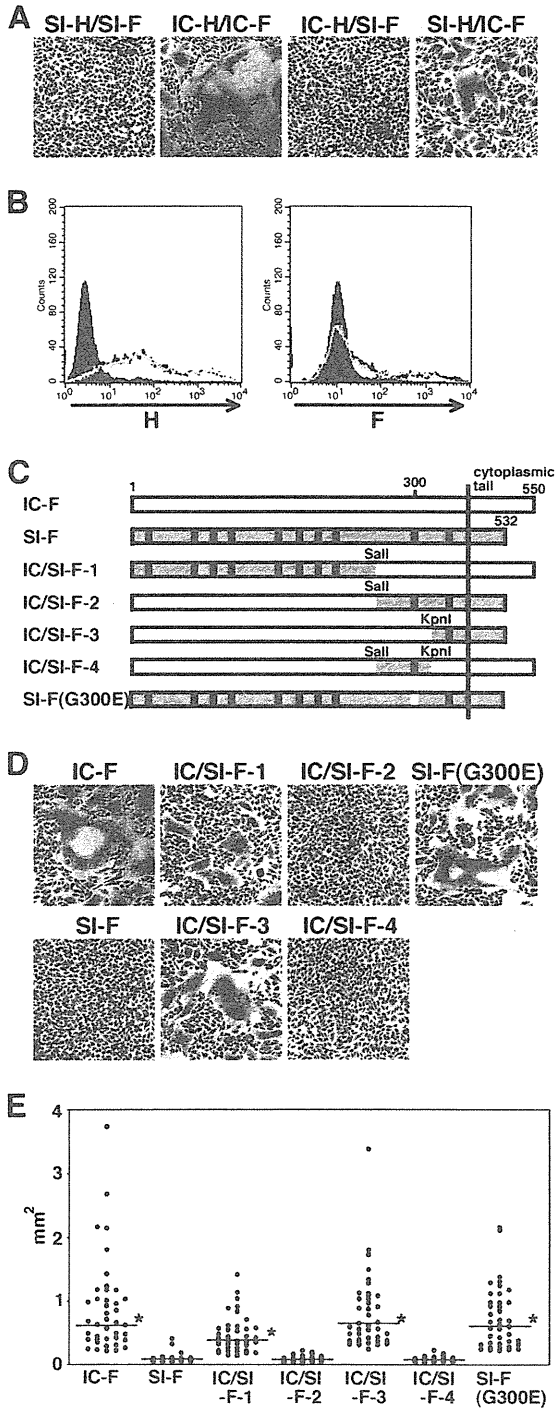

FIG. 6. Syncytium formation in cells expressing H and F proteins and identification of the amino acid residue in the F protein of the SI strain critical for reducing cell-to-cell fusion. (A) Syncytium formation in cells expressing H and F proteins of the IC-B or SI strains. CHO/hSLAM cells were transfected with a plasmid expressing the H protein of the IC-B or SI strain (IC-H or SI-H, respectively) together with a plasmid expressing the F protein of the IC-B or SI strain (IC-F or SI-F, respectively). At 24 h posttransfection, the cells were observed under a microscope after Giemsa staining. (B) Expression of the MV envelope proteins on the cells. CHO/hSLAM cells were transfected with a plasmid expressing IC-H, SI-H, IC-F, or SI-F. The cells expressing IC-H (black line) and SI-H (gray line) were stained with an anti-H protein MAb (left panel), and the cells expressing IC-F (black line) and SI-F (gray line) were stained with an anti-F protein MAb (right panel). All the cells were subsequently stained with an Alexa Fluor 488-conjugated secondary antibody. The cells without transfection were stained with an anti-H protein MAb or an anti-F protein MAb followed by an Alexa Fluor 488-conjugated secondary antibody (shaded regions). (C) Diagrams of the chimeric F proteins. There are 10 amino acid differences (shown by vertical lines) between IC-F and SI-F. The regions derived from SI-F are shaded, and those derived from IC-F are white. The restriction enzyme-replaced fragments are indicated. (D) Syncytium formation in cells expressing the chimeric or mutant F proteins. CHO/hSLAM cells were transfected with a plasmid expressing IC-H together with plasmids expressing IC-F protein, SI-F protein, chimeric F protein (IC/SI-F-1, -F-2, -F-3, or -F-4), or mutant SI-F protein (G300E). At 24 h posttransfection, the cells were observed under a phase-contrast imaging microscope after Giemsa staining. (E) Quantification of syncytium formation. CHO/hSLAM cells were transfected with IC-H-expressing plasmids and IC-F-, SI-F-, chimeric F-, or mutant F-expressing plasmids together with an mCherry-expressing plasmid. At 48 h posttransfection, areas of each syncytium with mCherry autofluorescence were measured using an Axio Observer.D1 microscope and ImageJ software. Forty syncytia were measured for each F protein. Asterisks indicate that the area of syncytia induced by IC-F, chimeric F, or mutant F was significantly larger than that induced by SI-F, based on the results of a t test ($P < 0.001$). The horizontal bars indicate the median values of the areas of syncytia.

teins) and nonstructural C and V proteins were well conserved in the SI strain (Table 1). We generated a recombinant MV possessing the IC323 genome in which the M, F, and H genes were replaced with those of the SI strain. The recombinant MV was designated IC/SI-MFH-AcGFP. The various types of cells shown in Fig. 4 were infected with IC/SI-MFH-AcGFP. IC/SI-MFH-AcGFP replicated poorly in SLAM- and ECR-positive cells and did not produce syncytia in these cells (Fig. 5A). A growth kinetics analysis of Vero/hSLAM cells, which were susceptible to all recombinant MVs, showed that IC/SI-MFH-AcGFP hardly produced cell-free viruses and exhibited a growth phenotype similar to that of SI-AcGFP (Fig. 4 and 5B). These data indicated that the membrane-associated protein-encoding genes (i.e., the M, F, and H genes) were responsible for the growth phenotype of the SI strain.

The E300G substitution in the F protein is responsible for the reduced membrane fusion activity. Previous papers have indicated that the typical changes in SSPE strains, namely, the lack of M protein expression and cytoplasmic tail truncation of the F protein, enhance the syncytium-forming activity of MV (6, 7). Indeed, other previous papers have shown high fusogenic activities of SSPE strains (1, 4, 8). Despite exhibiting the changes typical in SSPE strains, SI-AcGFP and IC/SI-MFH-AcGFP showed limited syncytium-forming activities (Fig. 4 and 5B). Using expression plasmids, the syncytium-forming activities of the H and F proteins of the SI strain were analyzed in CHO/hSLAM cells ($SLAM^+$). When the F protein of the SI strain (SI-F) was expressed together with the H protein of the SI strain (SI-H), no syncytia were detected (Fig. 6A; SI-H/SI-F). In contrast, many syncytia were observed when the F and H proteins of the IC-B strain (IC-F and IC-H, respectively) were expressed (Fig. 6A; IC-H/IC-F). Flow cytometry analyses indicated that the expression levels of SI-F and SI-H, respectively, were similar to those of IC-F and IC-H (Fig. 6B). The combination of SI-F and IC-H also showed poor syncytium-forming activity (Fig. 6A; IC-H/SI-F). On the other hand, when IC-F